Received: 18 February 2022 | Revised: 28 April 2022 | Accepted: 2 May 2022

DOI: 10.1002/cne.25345

RESEARCH ARTICLE

JCN RESEARCH IN SYSTEMS NEUROSCIENCE THE JOURNAL OF COMPARATIVE NEUROLOGY WILEY

The brain of the tree pangolin (*Manis tricuspis*). VII. The amygdaloid body

Aminu Imam[1,2] | **Adhil Bhagwandin**[1] | **Moyosore S. Ajao**[2] | **Paul R. Manger**[1]

[1]School of Anatomical Sciences, Faculty of Health Sciences, University of the Witwatersrand, Johannesburg, Republic of South Africa

[2]Department of Anatomy, Faculty of Basic Medical Sciences, College of Health Sciences, University of Ilorin, Ilorin, Nigeria

Correspondence
Paul Manger, School of Anatomical Sciences, University of the Witwatersrand, 7 York Road, Parktown, 2193, Johannesburg, South Africa.
Email: Paul.Manger@wits.ac.za

Associate Editor: Kathleen Rockland

Funding information
National Research Foundation-Third World Academy of Science African Renaissance Doctoral Fellowship (AI); the South African National Research Foundation (PRM)

Abstract

Here, we describe the cytoarchitecture and chemoarchitecture of the amygdaloid body of the tree pangolin. Our definition of the amygdaloid body includes the pallial portions of the amygdala, and the centromedial group that is a derivative of the subpallium and part of the extended amygdala. The remainder of the extended amygdala is not described herein. Within the amygdaloid body of the tree pangolin, we identified the basolateral group (composed of the lateral, basal, and accessory basal amygdaloid nuclei), the superficial, or cortical nuclei (the anterior and posterior cortical nuclei, the periamygdaloid cortex, and nuclei of the olfactory tract), the centromedial group (the central amygdaloid nucleus and the medial nuclear cluster), and other amygdaloid nuclei (the anterior amygdaloid area, the amygdalohippocampal area, the intramedullary group, and intercalated islands). The location within and relative to each other within the amygdaloid body and the internal subdivisions of these groups were very similar to that reported in other mammalian species, with no clearly derived features specific to the tree pangolin. The only variation was the lack of an insular appearance of the intercalated islands, which in the tree pangolin were observed as a continuous band of neurons located dorsomedial to the basolateral group similar in appearance to and almost continuous with the intramedullary group. In carnivores, the closest relatives of the pangolins, and laboratory rats, a similar appearance of portions of the intercalated islands has been noted.

KEYWORDS
affect, amygdala, behavior, Carnivora, emotion, Pholidota, RRID:AB_10000321, RRID:AB_10000323, RRID:AB_10000340, RRID:AB_10000343, RRID:AB_11204707, RRID:AB_2079751, RRID:AB_2088494, RRID:AB_2187552, RRID:AB_509997, RRID:AB_91545

Abbreviations: AAA, anterior amygdaloid area; ABi, accessory basal nucleus, intermediate part; ABmc, accessory basal nucleus, magnocellular part; ABpc, accessory basal nucleus, parvocellular part; ABsh, accessory basal nucleus, shell part; ac, anterior commissure; AHiA, amygdalohippocampal area; Bmc, basal nucleus, magnocellular part; Bi, basal nucleus, intermediate part; Bpc, basal nucleus, parvocellular part; CeC, central amygdaloid nucleus, capsular division; CeI, central amygdaloid nucleus, intermediate division; CeL, central amygdaloid nucleus, lateral division; CeM, central amygdaloid nucleus, medial division; CoA, anterior cortical amygdaloid nucleus; CoP, posterior cortical amygdaloid nucleus; I, intercalated island of the amygdala; LA, lateral amygdaloid nucleus; LAdl, lateral amygdaloid nucleus, dorsolateral part; LAm, lateral amygdaloid nucleus, medial part; LAvl, lateral amygdaloid nucleus, ventrolateral part; Mcd, medial amygdaloid nucleus, dorsal subdivision; Mcv, medial amygdaloid nucleus, ventral subdivision; N.Bas, nucleus basalis; NEO, neocortex; NLOT, nucleus of the lateral olfactory tract; OT, optic tract; P, putamen nucleus; PAC, periamygdaloid cortex; PACl, periamygdaloid cortex, lateral division; PACm, periamygdaloid cortex, medial division; PIR, piriform cortex; st, stria terminalis; STIA, bed nucleus of the stria terminalis, intraamygdaloid division; VP, ventral pallidum.

1 | INTRODUCTION

Pangolins are generally nocturnal, solitary animals, but there are a range of behaviors that have been observed in captive specimens that could be classified as affective. These include territorial marking, defensive behaviors and postures, vocalizations, aggression, as well as reproductive and social behaviors such as courtship, chasing, mounting, copulation, and maternal interactions (Mohapatra & Panda, 2014; Zhang et al., 2020). These behaviors are observed frequently across mammalian species and indicate that affective states and behaviors processed and initiated by the pangolin brain, specifically the amygdaloid complex, are likely the result of similarly organized circuits, albeit these circuits being refined in such a way as to process affect in a manner relevant to pangolin life history and the survival of individual pangolins as members of their species (Rolls, 1999; Sah et al., 2003; Panskepp, 2011).

The amygdaloid complex, composed of the amygdaloid body in the rostral pole of the temporal lobe and the extended amygdala within the subpallium, is known to be involved in the processing of rage/anger, fear/anxiety, and lust/sexuality (Pankseep, 2011). Understanding the consistencies and variations in the organization of the amygdaloid complex of mammals may provide insights into affective behaviors and how they may be altered as species traverse independent evolutionary trajectories or when they inhabit and adapt to different environments (Rubenstein & Wrangham, 2014). The majority of our knowledge of the structure and function of the amygdaloid complex has emerged from studies of laboratory rodents, primates, and humans (e.g., Krettek & Price, 1978; Price et al., 1987; Pitkänen & Amaral, 1993a, b; Pitkänen et al., 1997; Kemppainen & Pitkänen, 2000), with few studies providing detailed analyses of rarely or less frequently studied mammals (e.g., Limacher-Burrell, et al., 2016; Limacher-Burrell et al., 2018; Pillay et al., 2021).

The amygdaloid body within the brain of the tree pangolin occupies the rostral pole of the temporal lobe, a location typical for mammals, has a volume that would be expected for a mammal with a brain mass of around 10 g (Imam et al., 2017), and exhibits a distinct nucleus of the lateral olfactory tract (Imam et al., 2018a); however, no comprehensive reports of the internal organization are available for either the amygdaloid body or the subpallial located extended amygdala in this species. In the current study, we extend our observations on the anatomy of the central nervous system of the tree pangolin (Imam et al., 2017; Imam et al., 2018a, b; Imam et al., 2019a; Imam et al., 2019b; Imam et al., 2019c) by providing a detailed description of the nuclear and cortical organization of the amygdaloid body.

The amygdaloid complex of mammals contains both nuclear and cortical portions (within the amygdaloid body), as well as nuclei forming the extended amygdala (e.g., Alheid, 2003; de Olmos et al., 2004). Developmental gene expression studies have shown that the amygdaloid complex, the amygdaloid body and extended amygdala, derive from both pallial and subpallial domains, but in a complex manner (e.g., Puelles, 2017; Watson et al., 2017). In the current study, we describe the regions of the amygdaloid complex found within the rostral temporal pole (that we refer to as the amygdaloid body), including the nuclei forming the deep/basolateral group, the superficial/cortical-like/corticomedial nuclei, other amygdaloid nuclei (intramedullary group [IMG], amygdalohippocampal area [AHiA], intercalated cell masses [I], anterior amygdaloid area [AAA]), and the centromedial group. The regions assigned to the extended amygdala (apart from the centromedial group due to its topological continuity with pallial amygdala structures) such as the bed nuclei of the stria terminalis, shell of nucleus accumbens, and substantia innominata (Alheid, 2003) will be described in a subsequent article detailing the anatomy of the tree pangolin subpallial telencephalon.

2 | MATERIALS AND METHODS

2.1 | Specimens

Adult tree pangolins (*Manis tricuspis*), caught from wild populations in Esejire, Osun State, Nigeria, were used in the current study (see Imam et al., 2017, for full details of animals, permits, and collection and treatment of tissue). All animals were treated and used according to the guidelines of the University of the Witwatersrand Animal Ethics Committee (AESC No. 2012/53/01), which parallel those of the NIH for the care and use of animals in scientific experimentation. The tree pangolins were weighed and overdosed with weight appropriate doses of sodium pentobarbital (Euthanaze, 200 mg sodium pentobarbital/kg, i.p.). Once respiration had ceased, the animals were intracardially perfused, initially with a cold (4°C) rinse of 0.9% saline solution (0.5 L/kg body mass), followed by cold (4°C) 4% paraformaldehyde in 0.1M phosphate buffer solution (PB, pH: 7.4; 1 L/kg body mass). Following fixation, the brains were carefully removed from the skull and weighed. The tissue was post-fixed overnight (24 h) in 4% paraformaldehyde in 0.1 M PB at 4°C, and then allowed to equilibrate in 30% sucrose in 0.1 M PB at 4°C. The tissue was then transferred to an antifreeze solution (30% glycerol, 30% ethylene glycol, 30% distilled water, and 10% 0.244M PB) and kept at 4°C until it had equilibrated, and was then placed in a −20°C freezer for storage. In the current study, the brains of three of these tree pangolins (MT1, MT3, and MT5; see Imam et al., 2017) were sectioned, stained, and analyzed.

2.2 | Sectioning and immunohistochemical staining

Prior to sectioning, each brain was allowed to equilibrate in 30% sucrose in 0.1 M PB at 4°C. The brains were then frozen in crushed dry ice and sectioned into 50-μm-thick sections on a freezing microtome. The whole brain of MT1 was sectioned in the coronal plane and a one in 10 series of sections taken and stained for Nissl, myelin, tyrosine hydroxylase (TH), orexin-A (OxA), serotonin (5HT), parvalbumin (PV), calbindin (CB), calretinin (CR), neurofilament H (NFH), and vesicular glutamate transporter 2 (vGlut2). The whole brain of MT3 was sectioned in the coronal plane and a one in five series of sections taken and stained for neuronal nuclear marker (NeuN), choline acetyltransferase (ChAT), PV, CB, and CR. The right half of the brain of MT5 was

TABLE 1 Sources and dilution of antibodies used in the current study

Antibody	Host	Immunogen	Manufacturer	Catalogue No.	Reference	Dilution	RRID
ChAT	Goat	Human placental enzyme	Merck-Millipore	AB144P	Laux et al. (2012); Kaiser et al. (2011)	1:3000	AB_2079751
TH	Rabbit	Purified tyrosine hydroxylase from rat adrenal	Merck-Millipore	AB151	Piskuric et al. (2011)	1:3000	AB_10000323
OxA	Rabbit	Synthetic peptide corresponding to the c-terminal portion of bovine orexin-A peptide	Merck-Millipore	AB3704	Li and Kiruoac (2008)	1:3000	AB_91545
5HT	Rabbit	Serotonin covalently bound to bovine thyroglobulin with carbodiimide	Merck-Millipore	AB938	Not available	1:5000	Not available
PV	Rabbit	Rat muscle parvalbumin	Swant	PV28	Hirano et al. (2011)	1:10,000	AB_10000343
CB	Rabbit	Rat recombinant calbindin D-28k	Swant	CB38a	Bunce et al. (2013)	1:10,000	AB_10000340
CR	Rabbit	Recombinant human calretinin containing a 6-his tag at the N-terminal	Swant	7699/3H	Adrio et al. (2011)	1:10,000	AB_10000321
vGlut2	Mouse	Recombinant protein from rat vGlut2	Merck-Millipore	MAB5504	Wong et al. (2008); Griffin et al. (2010)	1:4000	AB_2187552
SMI-32	Mouse	Nonphosphorylated epitope of neurofilament H from rat hypothalami	Covance	SMI-32R	Sternberger and Sternberger (1983)	1:1000	AB_509997
NeuN	Rabbit	GST-tagged recombinant protein corresponding to mouse NeuN	Merck-Millipore	ABN78C3	Ngwenya et al. (2016)	1:500	AB_11204707
DCX	Goat	c-Terminus of doublecortin of human origin	Santa Cruz Biotechnology	sc-8006	Brown et al. (2003); Patzke et al. (2015)	1:300	AB_2088494

sectioned in the sagittal plane and a one in 10 series of sections taken and stained for Nissl, myelin, TH, 5HT, PV, CB, CR, NFH, vGlut2, and doublecortin (DCX). Complete details of staining for Nissl and myelin, antibody characterization, specificity, and the protocol followed for all immunostains listed above, have been provided previously (Imam et al., 2018a; but see Table 1 for antibody details).

2.3 | Analysis and iconography

A low power stereomicroscope was used to examine the sections and camera lucida drawings outlining architectural borders were made. Architectonic borders of the amygdaloid nuclei and cortical regions were first defined using the standard Nissl and myelin stains. The parcellation of the nuclear and cortical regions of the amygdaloid body was then confirmed and refined using the immunohistochemical stains. The drawings were then scanned and redrawn using the Canvas Draw 6 drawing program (Canvas GFX, Inc., FL, USA). The nomenclature used in the current study was based primarily on that used by Paxinos et al. (2009), Price et al. (1987), Sah et al. (2003), Radtke-Schuller (2018), and Pillay et al. (2021). While amygdaloid terminology varies across studies and species (e.g., Sorvari, Soininen et al., 1995; Pillay et al., 2021), where the terminology used in these studies was not appropriate to the current findings, we used the most appropriate terminology available. Digital photomicrographs were captured using an Axiocam 208 color camera mounted to a Zeiss Axioskop microscope (with Zeiss A-Plan 5X/012, Zeiss Plan-NeoFluar 10X/0.30, and Zeiss Plan-NeoFluar 40X/0.75 objectives). No pixilation adjustments, or manipulation of the captured images were undertaken, except for the adjustment of contrast, brightness, and levels using Adobe Photoshop.

3 | RESULTS

In the tree pangolin, the amygdaloid body, as noted previously (Imam et al., 2017), was observed in the rostral aspect of the temporal portion, or lobe, of the cerebral hemisphere (Figures 1 and 2). Within the amygdaloid body, we identified four major groups including the basolateral (or deep) group (or complex), the superficial (or cortical-like, or corticomedial) nuclei, the centromedial group, and other amygdaloid nuclei (Figure 2). As mentioned, the current study only describes the nuclei and cortical areas of the amygdaloid complex found in the rostral

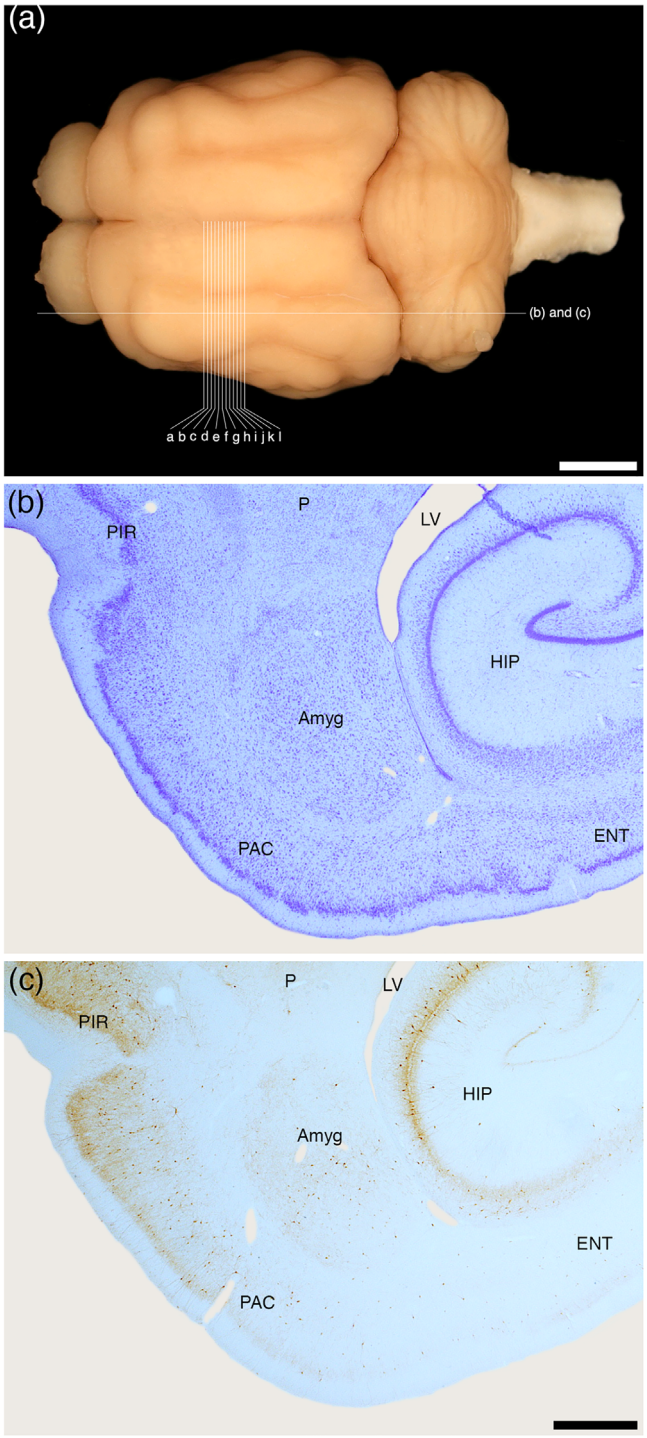

FIGURE 1 (a) Photograph of the dorsal surface of the tree pangolin brain showing the approximate sagittal plane of the sections depicted in (b) and (c) of this figure, and the approximate coronal planes of the Diagrams (a)–(l) of Figure 2. Scale bar in (a) = 5 mm. Photomicrographs of sagittal (b) Nissl-stained and (c) parvalbumin immunostained sections through the amygdaloid body (Amyg) of the tree pangolin showing the topological relationships of this structure within the brain of this species. In all images, rostral is to the left, and in (b) and (c) dorsal to the top of the image. Scale bar in (c) = 1 mm and applies to (b) and (c). See list for abbreviations

temporal region, which we refer to as the amygdaloid body. We note here that the development of the amygdala is very complex and that our assignation of structures as belonging to the "amygdaloid body" may need to be altered, as portions (such as the centromedial group) may be assigned to the extended amygdala (Alheid, 2003; de Olmos et al., 2004).

3.1 | Deep or basolateral group/complex

The basolateral group was composed of three nuclei, the lateral, basal, and accessory basal amygdaloid nuclei (Figures 2 and 3). The basolateral group occupied the majority of the amygdaloid body and could be readily delineated from the other parts of the amygdaloid body and adjacent nonamygdaloid structures with the range of stains used in the current study (Figure 3).

3.1.1 | The lateral amygdaloid nucleus of the basolateral group

The lateral amygdaloid nucleus (LA) occupied the dorsolateral most aspect of the basolateral group (Figures 2(b)–2(k)) and was readily differentiated from the other nuclei of the basolateral group by the relatively low intensity neuropil staining for choline acetyltransferase and calbindin (Figures 3(c) and 3(e)). The LA was composed of three distinct parts, the dorsolateral part (LAdl), the medial part (Lam), and the ventrolateral part (LAvl), although the distinction of these parts from each other was not always straightforward. The neuronal types observed in each of the three parts appeared similar, although the packing density of larger neurons in the LAdl appeared slightly higher than the LAm and LAvl, and the LAvl appeared to have a slightly higher packing density of smaller neurons than the LAm and LAdl (Figure 3(a)). A low density of myelinated fibers was observed in all three parts, but a mediolaterally oriented fiber band appeared to distinguish the LAdl from the LAm and LAvl (Figure 3(b)). While the light, diffuse staining for choline acetyltransferase was very pale and similar across the three parts (Figure 3(c)), similar staining for parvalbumin appears slightly more intense in the LAdl compared with both the Lam and Lavl (Figure 3(d)). Larger multipolar parvalbumin-immunopositive neurons were observed in the LAdl, whereas in both the LAm and LAvl, a lower density of smaller, multipolar parvalbumin-immunopositive neurons was observed (Figures 3(d) and 3(h)). Very few scattered calbindin-immunopositive neurons were observed in the LAm and LAvl, but these were clearly more numerous in the LAdl (Figure 3(e)).

3.1.2 | The basal amygdaloid nucleus of the basolateral group

The basal amygdaloid nucleus occupied the middle portion of the basolateral group (Figures 2(c)–2(k)), and was divisible into magnocellular (Bmc), intermediate (Bi), and parvocellular (Bpc) parts (Figures 2

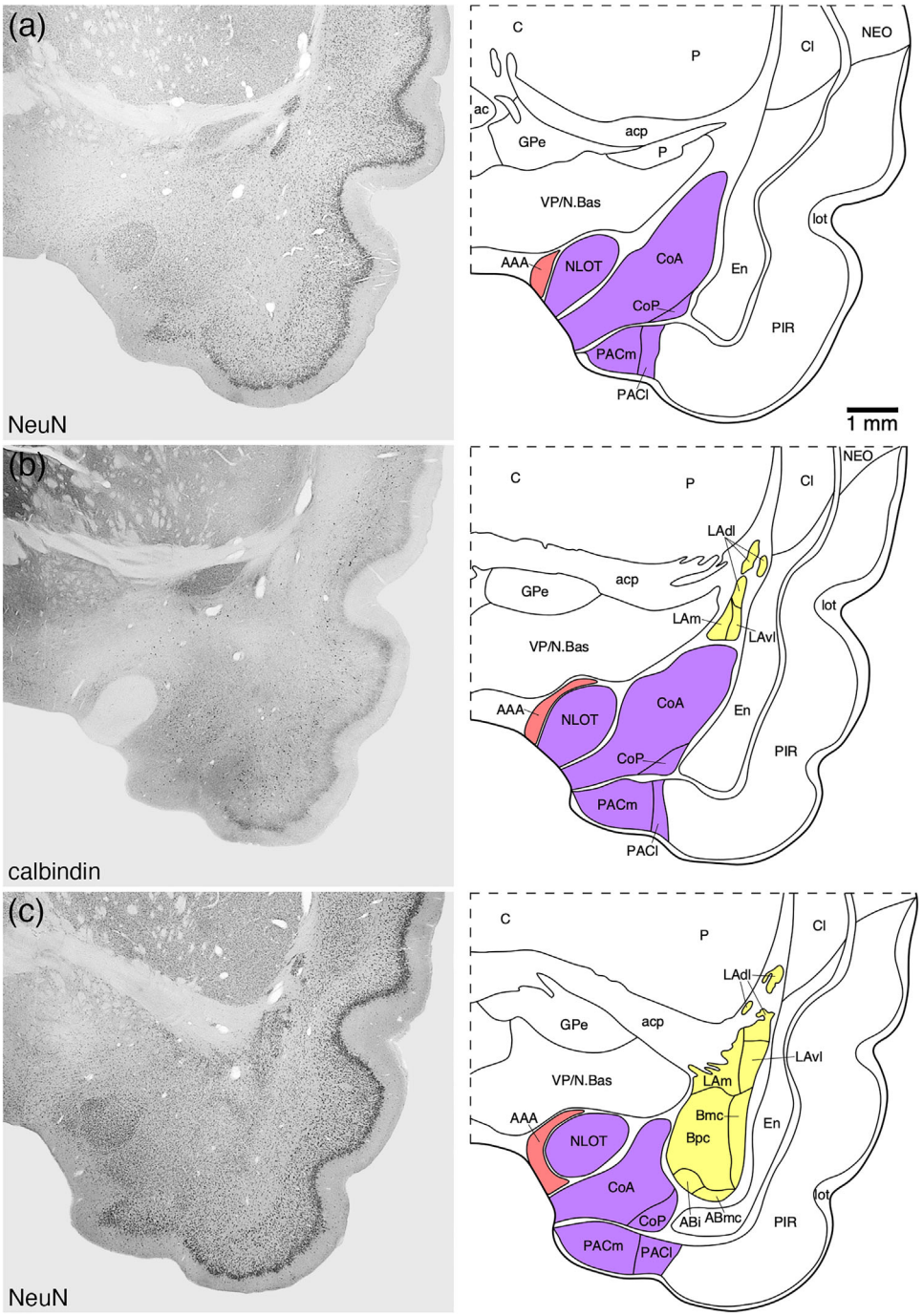

FIGURE 2 Representative photomicrographs and associated diagrammatic reconstructions showing the nuclear and cortical organization of the amygdaloid body of the tree pangolin. The photomicrographs are of coronal sections immunostained for neuronal nuclear marker (NeuN, a, c, e, g, j, k, l), parvalbumin (f), calbindin (b, h), and calretinin (d, i). The associated diagrams are from the same series of sections from which the photomicrographs were taken, but represent the combined architectural analysis from all sections, as compared to the single representation shown in the photomicrographs. In all photomicrographs and diagrams, dorsal is to the top and medial to the left. Photomicrograph and diagram (a) represent the most rostral portion of the amygdaloid body, while photomicrograph and diagram (l) represent the most caudal portion. Each photomicrograph and diagram are approximately 250 μm apart. The various nuclear/cortical groups of the amygdaloid body are represented with differing colors, including the deep or basolateral group in yellow, the superficial or cortical-like or corticomedial group in purple, the centromedial group in green, and the remaining amygdaloid nuclei in red. See list for abbreviations

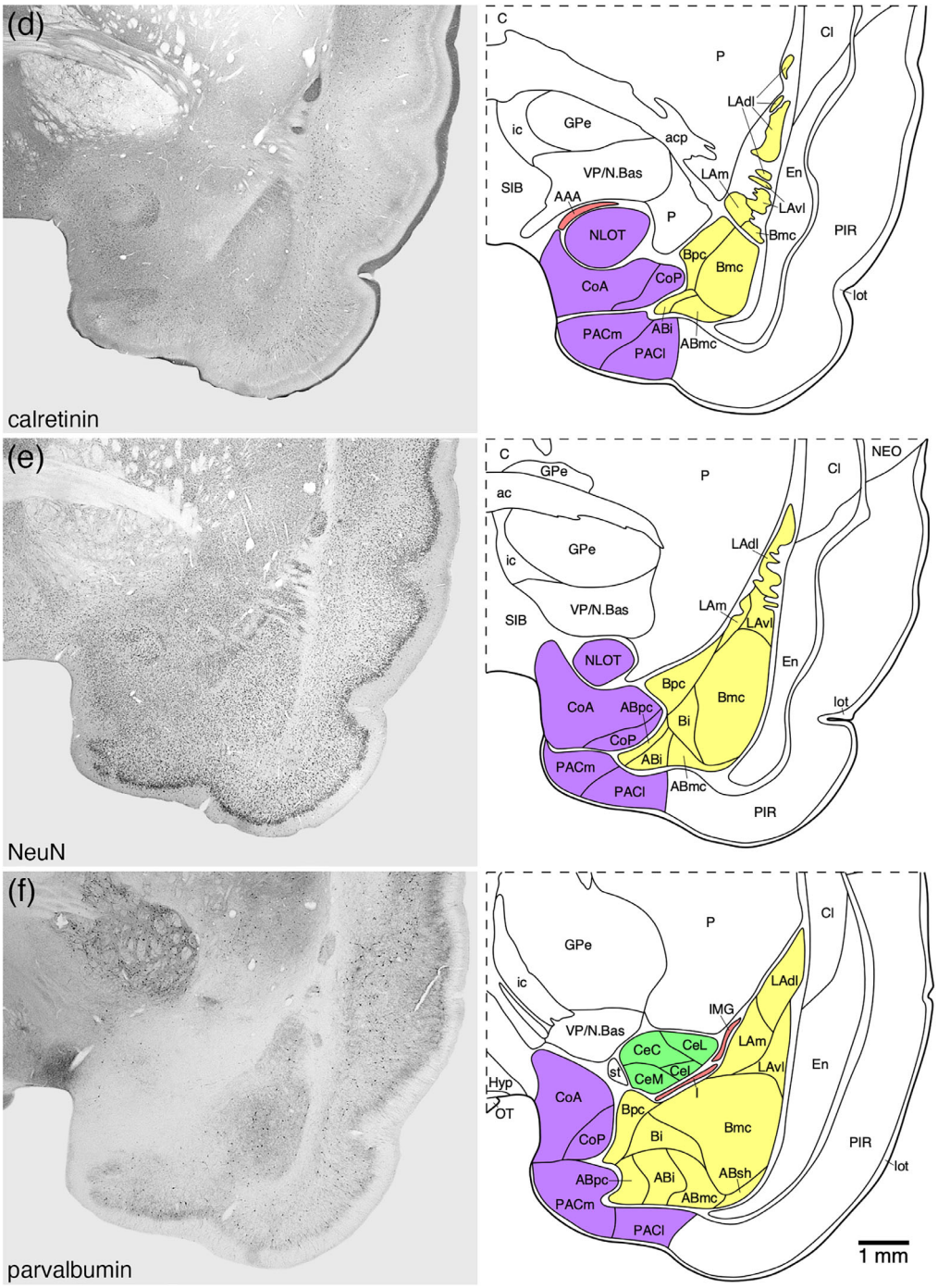

FIGURE 2 Continued

and 3). The largest and most distinct of these parts was the Bmc, which was located dorsally within the nucleus and was composed of relatively larger neurons than the Bi and Bpc and the dorsally adjacent LA (Figures 3(a) and 3(f)); with the relatively smaller neurons occupying the Bpc distinguishing this part from the slightly larger neurons of the Bi (Figure 3(a)). In addition, fascicles of myelinated fibers were observed to course through the Bmc, with a lower density of these fascicles in the Bi and their near absence from the Bpc (Figure 3(b)). One of the distinguishing features of the Bmc was the presence of an intense choline acetyltransferase-immunopositive neuropil staining that was absent in both the Bi and Bpc and the LA (Figure 3(c)). A moderately intense parvalbumin-immunopositive neuropil staining distinguished the basal amygdaloid nucleus from the lateral and accessory basal nuclei (Figure 3(d)), with larger, multipolar parvalbumin-immunopositive neurons being located within the Bmc, smaller parvalbumin-immunopositive neurons in the Bpc, and a paucity of parvalbumin-immunopositive neurons in the Bi (Figure 3(d)). The density and distribution of calbindin-immunopositive neurons and

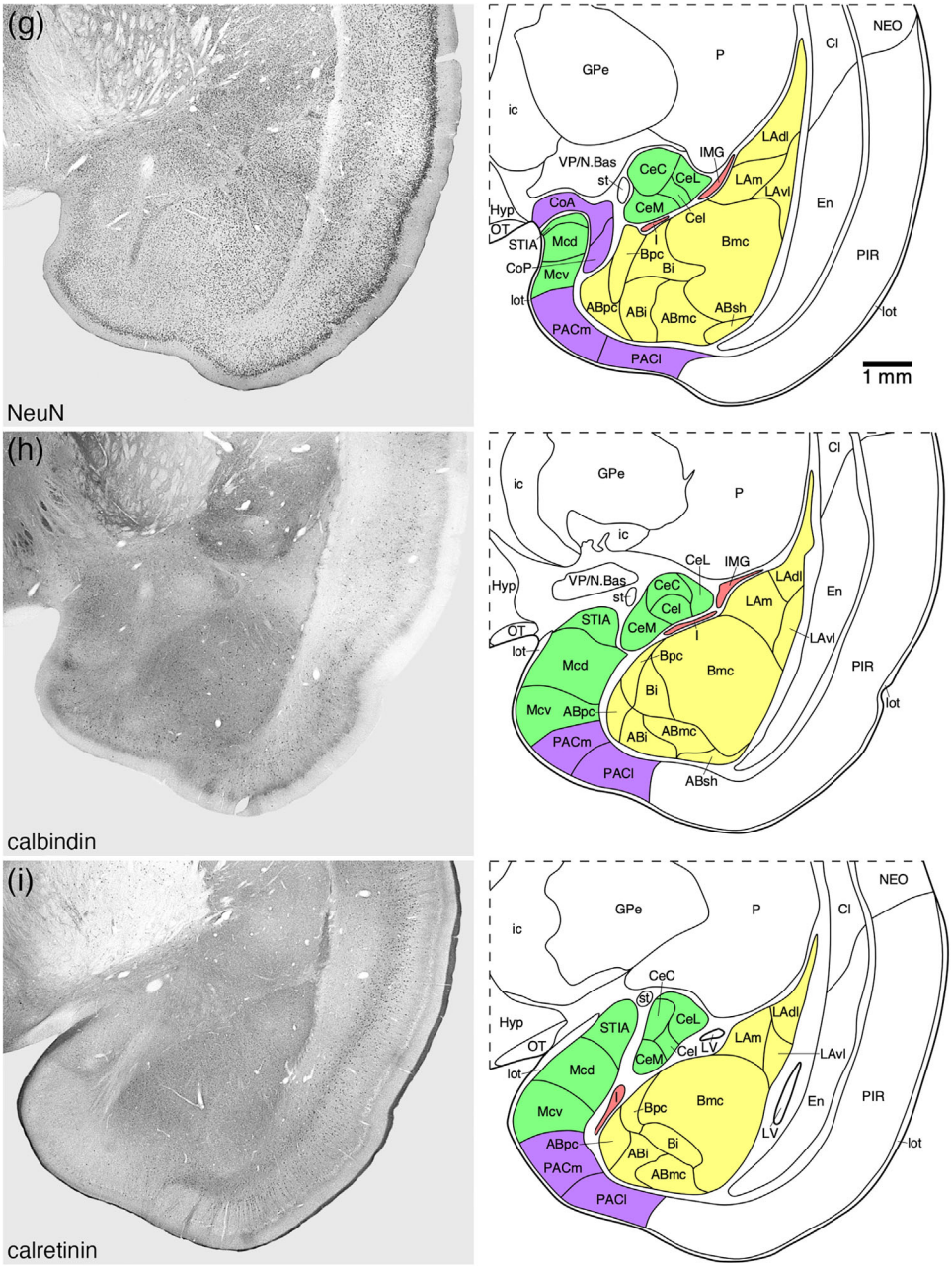

FIGURE 2 Continued

calbindin-immunopositive neuropil staining was similar across the three parts of the basal amygdaloid nucleus (Figure 3(e)).

3.1.3 | The accessory basal nucleus of the basolateral group

The accessory basal amygdaloid nucleus occupied the ventral most aspect of the basaolateral group and could be divided into four parts, magnocellular (ABmc), intermediate (Abi), parvocellular (Abpc), and shell (Absh) parts (Figures 2(c)–2(j) and 3). Due to the moderate density of larger relative soma sizes of the neurons, the ABmc was the most readily identified part of this nucleus (Figures 3(a) and 4). The ABi had slightly smaller neurons than those of the ABmc, with those of the ABpc being smaller than those of the ABi, while those in the ABsh were smaller than the ABmc neurons and exhibited a slightly higher packing density (Figures 3(a) and 4(a)). Across the four parts, we observed a consistent low density of myelinated fibers (Figures 3(b) and 4(b)). This consistency was maintained when observing immunoreactive neurons for parvalbumin and calbindin (Figures 3(d), 3(e), 3(g), 4(c), and 4(d)), and neuropil immunoreactivity for choline acetyltransferase, parvalbumin, and calbindin (Figures 3(c)–3(e), 4(c), and 4(d)). Thus, the four parts of the accessory basal nucleus of the basolateral group in the tree pangolin brain are most clearly distinguished cytoarchitecturally.

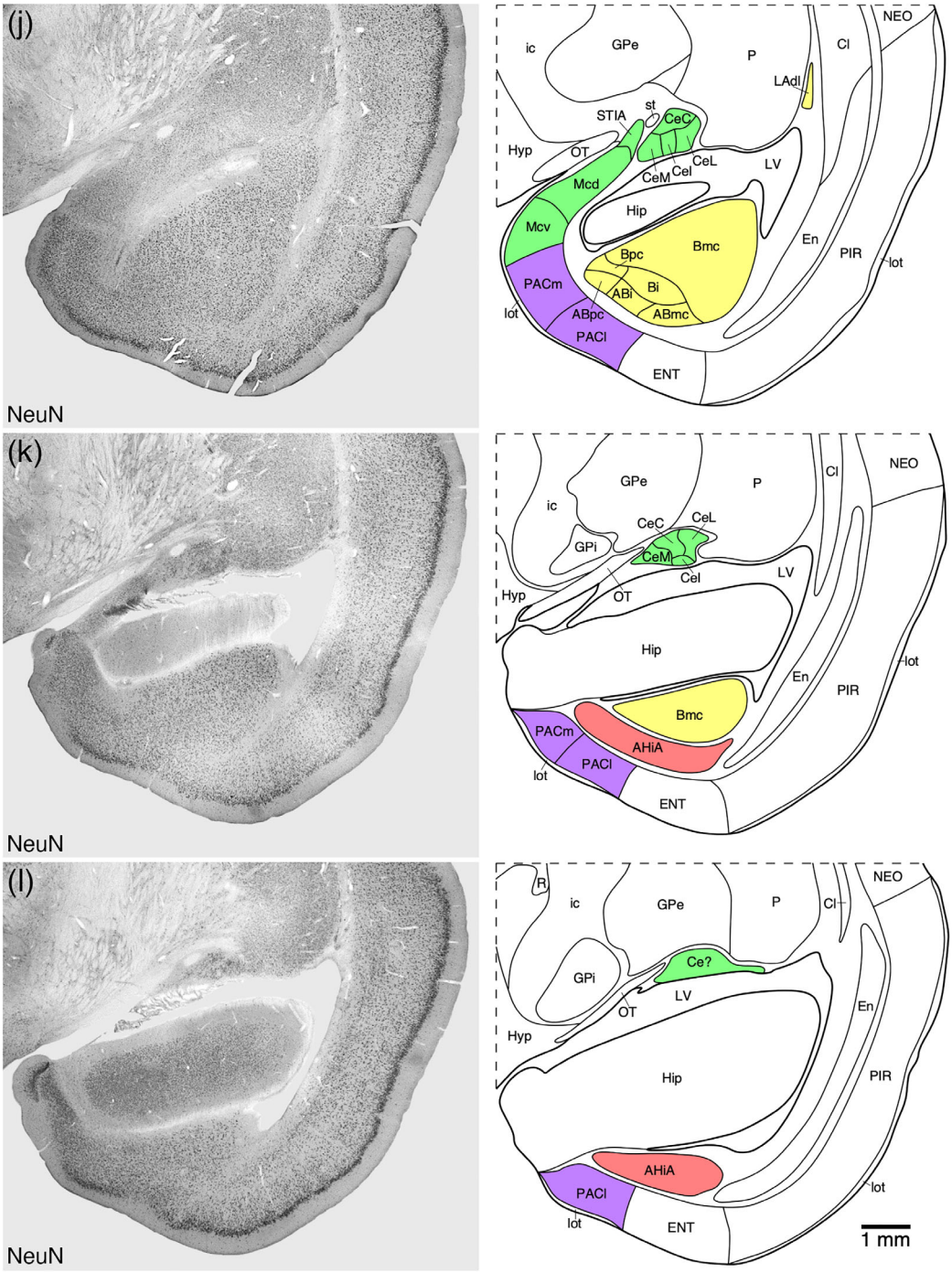

FIGURE 2 Continued

3.2 | Superficial or cortical-like or corticomedial nuclei

The nuclei or cortical areas that are assigned to the superficial nuclei usually comprise the nuclei of the lateral (NLOT) and accessory (NAOT) olfactory tracts, the anterior and posterior cortical nuclei, and the peri-amygdaloid cortical areas. Both the NLOT (Figures 2(a)–2(e) and 5) and NAOT have been described previously (Imam et al., 2018a) and are thus not considered further herein.

3.2.1 | The anterior and posterior cortical nuclei

Distinct anterior (CoA) and posterior (CoP) cortical nuclei were located in the ventral aspect of the rostromedial region of the amygdaloid body (Figures 2(a)–2(g)). The CoA was the larger and more rostromedially located of the two nuclei and was composed of a moderate to high density of relatively smaller neurons (Figure 5(a)). The soma of the neurons forming the CoP were larger than those of the CoA and were present in a lower density than the neurons of the CoA (Figure 5(a)).

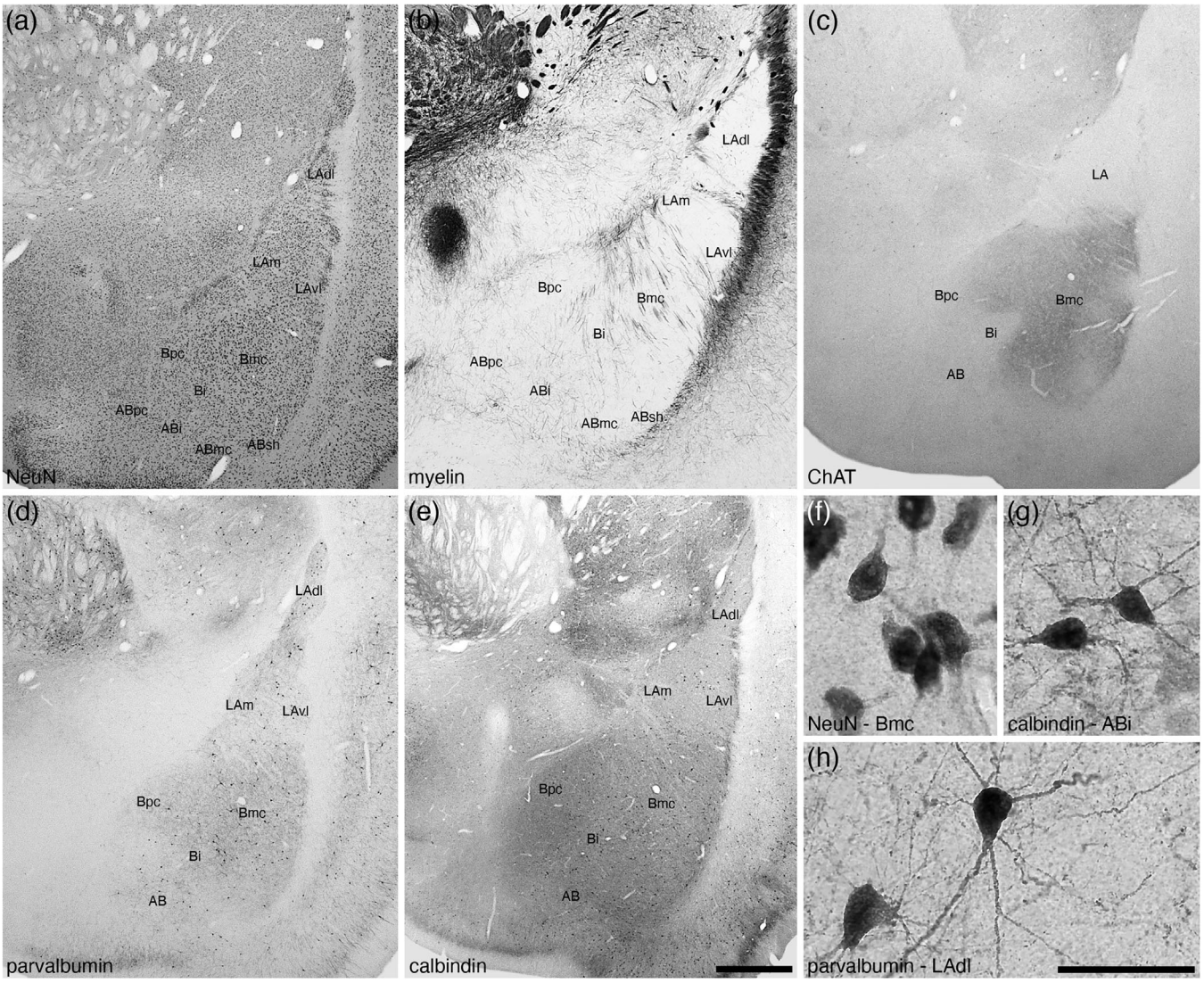

FIGURE 3 Low (a–e) and high (f–h) magnification photomicrographs of the basolateral nuclear complex within the amygdaloid body of the tree pangolin stained for neuronal nuclear marker, NeuN (a, f), myelin (b), cholineacetyltransferase, ChAT (c), parvalbumin (d, h), and calbindin (e, g). Within the lateral amygdaloid nucleus (LA), we identified the dorsolateral (LAdl), medial (LAm), and ventrolateral (LAvl) parts. Within the basal amygdaloid nucleus, we identified the magnocellular (Bmc), intermediate (Bi), and parvocellular (Bpc) divisions, and within the accessory basal nucleus (AB), we identified the intermediate (ABi), magnocellular (ABmc), parvocellular (ABpc), and shell (ABsh) divisions. Certain stains were specific to particular nuclei, such as the intense ChAT neuropil staining (c) in the Bmc. Images (f) and (g) show examples of neural morphology in the (f) Bmc, NeuN immunostaining, (g) ABi, calbindin immunostaining, (h) LAdl, parvalbumin immunostaining. In all images, dorsal is to the top and medial to the left. Scale bar in (e) = 1 mm and applies to (a)–(e). Scale bar in (h) = 250 μm and applies to (f)–(h). See list for abbreviations

A low to moderate density of myelinated fibers was observed in both nuclei (Figure 5(b)). Within the CoA, scattered multipolar neurons immunopositive for parvalbumin was observed, but a low to moderate density of these neurons was observed in the CoP (Figure 5(c)). While there was clear parvalbumin-immunopositive dendritic networks in both nuclei, the density of these networks was higher in the CoP than the CoA (Figure 5(c)). Calbindin-immunopositive neurons and neuropil staining was noted in both nuclei, although these immunopositive neurons exhibited slightly smaller soma and were in a higher density in the CoA compared with the CoP (Figure 5(d)).

3.2.2 | The periamygdaloid cortex

The periamygdaloid cortex, located in the ventral most aspect of the amygdaloid body, was composed of medial (PACm) and lateral (PACl) periamygdaloid cortical areas (Figure 2). Both areas were composed of a three-layered cortex, including a distinct neuron-sparse molecular layer (layer 1, bordered externally by the lateral olfactory tract), a neuron dense layer 2, and a less neuron dense layer 3 (Figures 6(a), 6(e), and 6(j)). Layer 1 in both the PACm and PACl contained a low density of scattered neurons, a low density of parvalbumin-immunopositive apical dendrites, a low density calbindin- and calretinin-immunopositive

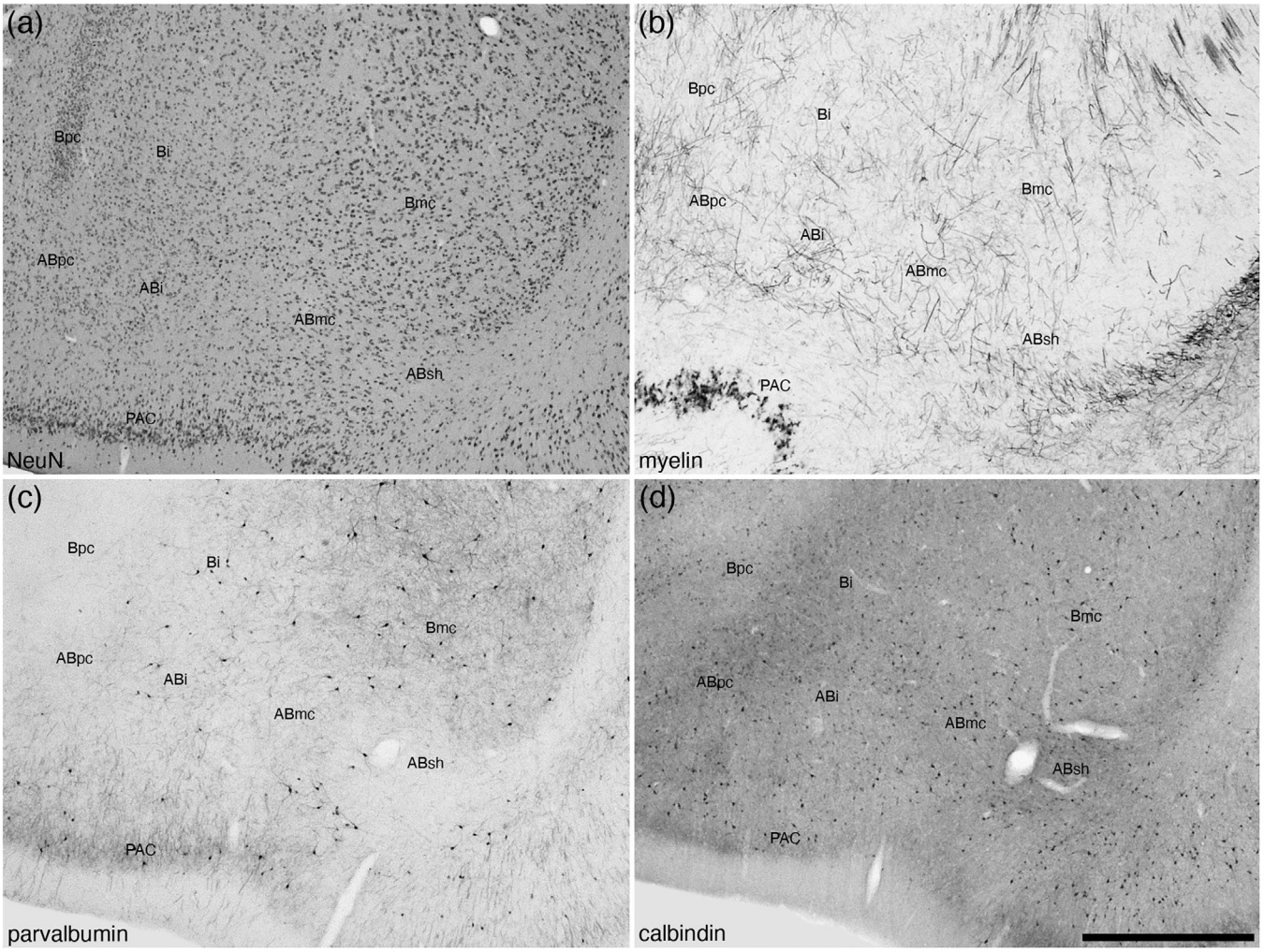

FIGURE 4 Low magnification photomicrographs of the accessory basal amygdaloid nucleus (AB) within the amygdaloid body of the tree pangolin stained for neuronal nuclear marker, NeuN (a), myelin (b), parvalbumin (c), and calbindin (d). Note that only subtle variations exist between the parts of this nucleus, the magnocellular (ABmc), intermediate (ABi), parvocellular (ABpc) and shell (ABsh) parts, with the cytoarchitecture as revealed with NeuN (a) immunostaining being the most reliable stain for identification of these parts. In all images, dorsal is to the top and medial to the left. Scale bar in (d) = 1 mm and applies to all. See list for abbreviations

terminal network, and an absence of structures immunopositive for neurofilament H (Figure 6). Layer 2 in both areas contained the highest density of neurons, although the packing density in the PACm appears slightly higher than in the PACl (Figures 6(a), 6(e), and 6(j)). In both areas, a low density of parvalbumin-immunopositive neurons were noted, and the density of parvalbumin-immunopositive structures in layer 2 appears higher in the PACl when compared with the PACm (Figures 6(b), 6(f), and 6(k)). In layer 2 of the PACm, very few calbindin-immunopositive neurons were observed, with these being more numerous in PACl, with some of these neurons being relatively large multipolar neurons (Figures 6(c), 6(g), and 6(l)). In contrast, the density of the calbindin-immunopositive terminal network in the PACm appeared higher in the PACm compared with the PACl (Figures 6(c), 6(g), and 6(l)). A few scattered, small calretinin-immunopositive neurons were observed in layer 2 of the PACm, but these were not readily observed in the PACl (Figures 6(d), 6(h), and 6(i)). A similar density of neurofilament H-immunopositive dendrites were observed in layer 2 of both areas (Figures 6(i) and 6(n)). A similar low to moderate density of neurons of various shapes and sizes was observed in layer 3 of both cortical areas (Figures 6(a), 6(e), and 6(j)), with layer 3 of both areas containing a low density of parvalbumin-immunopositive neurons (Figures 6(b), 6(f), and 6(k)). Very few small, palely stained, calbindin-immunopositive neurons were observed in layer 3 of PACm, whereas a higher density of more intensely stained calbindin-immunopositive neurons were observed in layer 3 of PACl (Figures 6(c), 6(g), and 6(l)). A low density of palely stained, calretinin-immunopositive neurons was observed in layer 3 of the PACm, whereas no similar neurons were observed in the PACl. Neurofilament H immunostaining revealed a low density of stained neurons in layer 3 of the PACl, whereas in the PACm only immunostained dendrites were observed (Figures 6(i) and 6(n)). These similarities and differences allowed the delineation of these two cortical areas, from each other and the adjacent cortical territories.

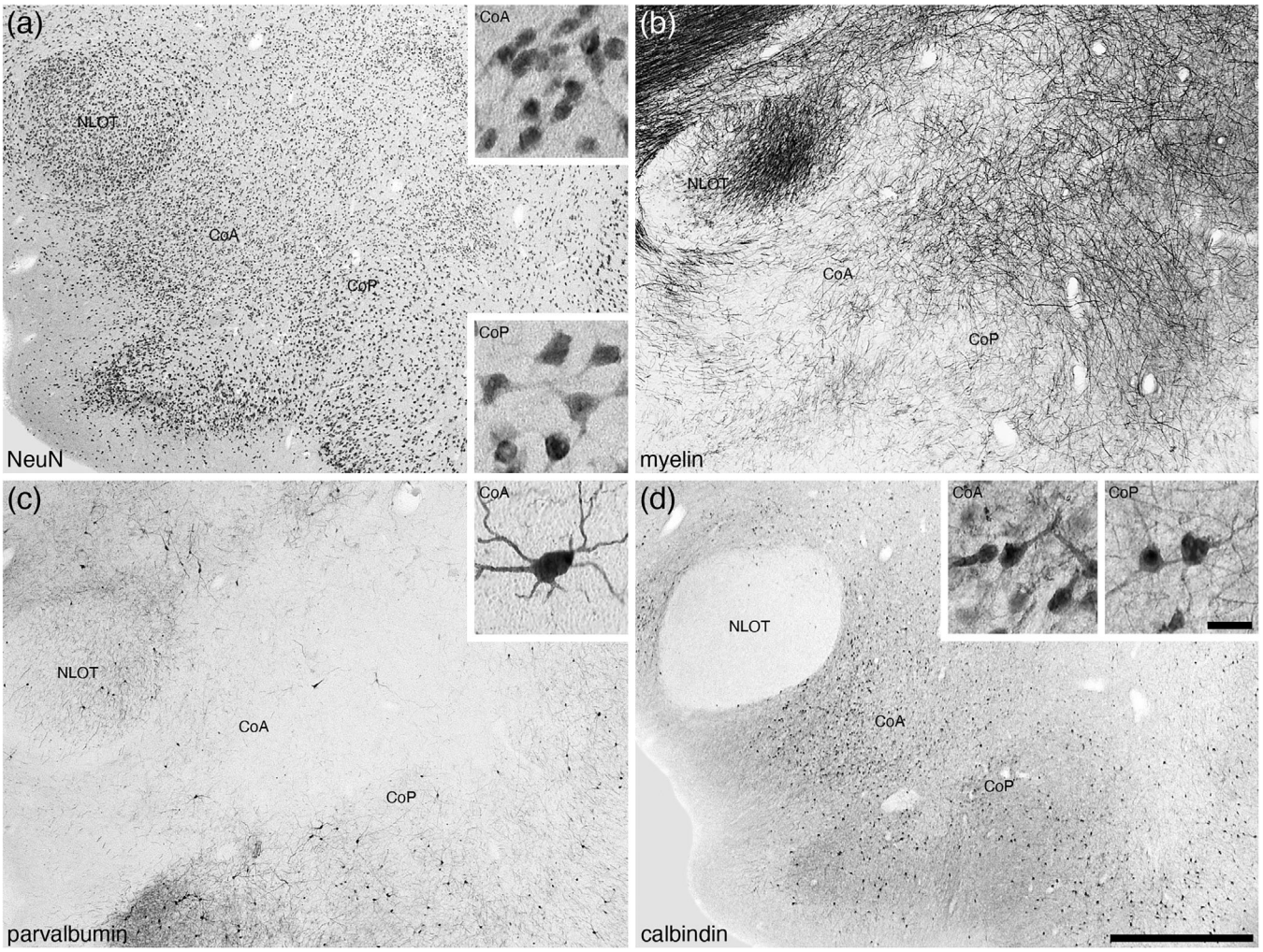

FIGURE 5 Low (a–d) and high (insets in a, c, d) magnification photomicrographs of the anterior (CoA) and posterior (CoP) cortical amygdaloid nuclei of the amygdaloid body of the tree pangolin stained for neuronal nuclear marker, NeuN (a), myelin (b), parvalbumin (c), and calbindin (d). Note the presence of larger neurons, increased myelin density, occasional parvalbumin immunostained neurons, and lower density of calretinin immunopositive structures in the CoP compared with the CoA. The insets in a, c, d are high magnification images of NeuN (a), parvalbumin (c), and calbindin (d) stained neurons in the CoA and CoP. In all images, dorsal is to the top and medial to the left. Scale bar in (d) = 1 mm and applies to (a)–(d). Scale bar in inset (d) = 25 μm and applies to all insets. See list for abbreviations

3.3 | Centromedial group

The centromedial group of the amygdaloid body of the tree pangolin was composed of the central amygdaloid nucleus, the bed nucleus of the stria terminalis, intraamygdaloid division (STIA), and the medial nuclear cluster. The centromedial group was located in the dorsomedial aspect of the amygdaloid body of the tree pangolin brain (Figures 2(f)–2(l)).

3.3.1 | The central amygdaloid nucleus

The central amygdaloid nucleus was composed of four divisions, the capsular (CeC), intermediate (CeI), lateral (CeL), and medial (CeM) divisions, although the delineation of these divisions was not always particularly clear (Figures 2(f)–2(l) and 7). In the CeC, CeL, and CeM divisions, a moderate density of neurons was observed, although in the CeI, the neuronal density appeared lower than in the other divisions (Figure 7(a)). In both the CeC and CeL, a slightly higher density of myelinated fibers was observed compared with the CeM, while the CeI exhibited the lowest density of myelinated fibers (Figure 7(b)). A low density of calbindin-immunpositive neurons were observed in the CeC, CeL, and CeM, but in the CeI, only a few scattered calbindin-immunpositive neurons were observed (Figure 7(c)). In both the CeL and CeM, a moderately intense neuropil immunostaining for calbindin was present, the intensity of which was lower in the CeC and lowest in the CeI (Figure 7(c)). The highest density of neurofilament H-immunopositive structures were observed in the CeC and CeL, with a lower density being observed in the CeM and the lowest density in the CeI (Figure 7(d)). The remaining stains used in the current

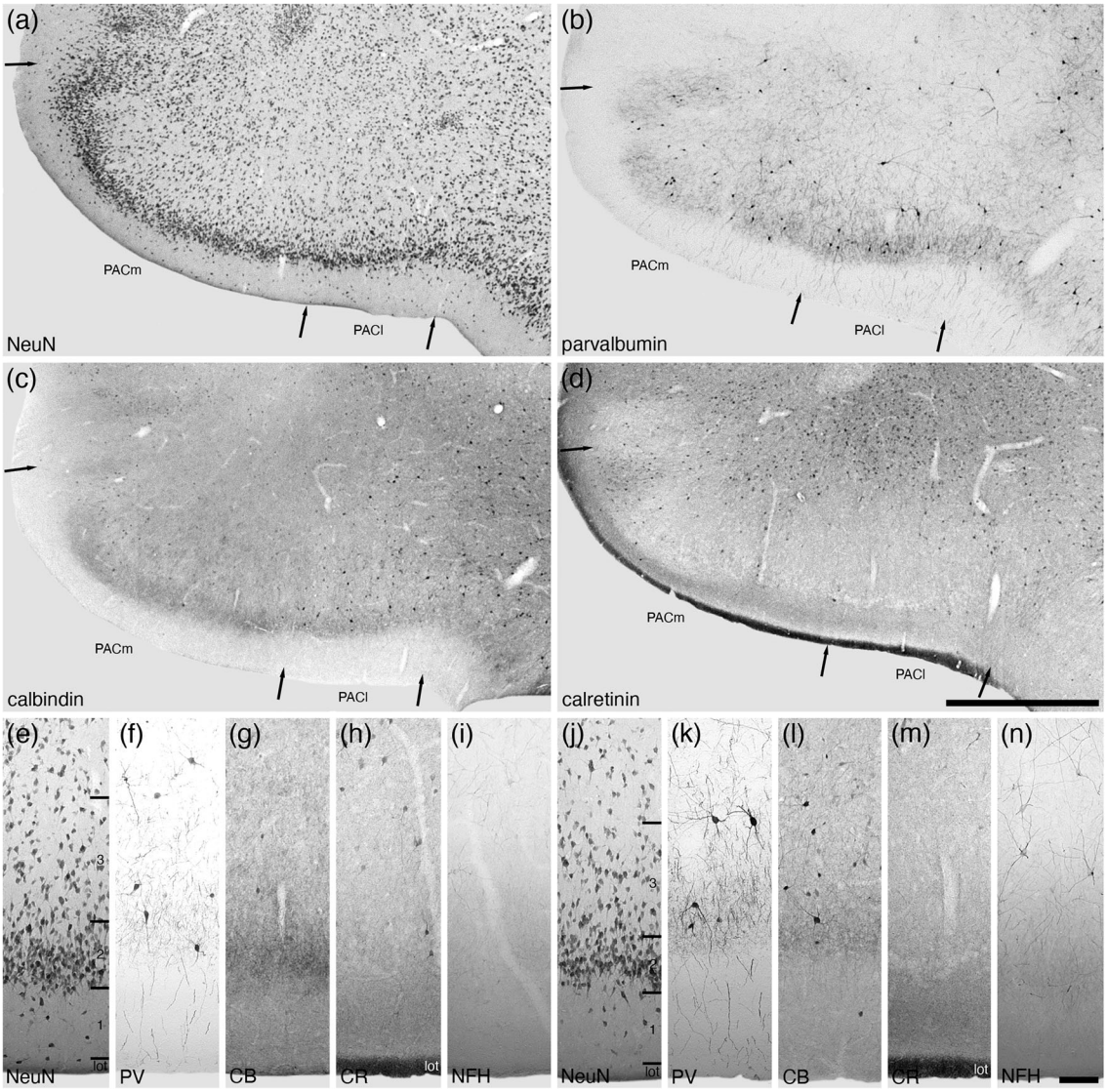

FIGURE 6 Lower (a–d) and higher (e–n) magnification photomicrographs of the periamygdaloid cortex (PAC) within the amygdaloid body of the tree pangolin stained for neuronal nuclear marker (NeuN, a, e, j), parvalbumin (PV, b, f, k), calbindin (CB, c, g, l), calretinin (CR, d, h, m), and neurofilament H (NFH, i, n). Both the medial (PACm, e–i) and lateral (PACl, j–n) periamygdaloid cortical areas exhibit a trilaminate organization (layers 1, 2, 3). In all images, dorsal is to the top and medial to the left. Scale bar in (d) = 1 mm and applies to a–d. Scale bar in (n) = 100 μm and applies to (e)–(n). See list for abbreviations

study showed no differentiation between the divisions, but using the variances noted we could postulate the presence of and delineate these four divisions.

3.3.2 | The STIA

The small STIA was located on the most dorsal aspect of the medial cortical region of the amygdaloid body of the tree pangolin (Figures 2(g)–2(j)). This division evinced a weakly defined bilaminar appearance, with a superficial lamina composed of a lower density of larger neurons, while a higher density of smaller neurons comprised the deeper lamina (Figure 8(a)). No parvalbumin- or neurofilament H-immunoreactive structures were observed in the STIA (Figures 8(d) and 8(g)), with calbindin-immunopositive neurons being found primarily in the deeper lamina (Figure 8(e)) and calretinin-immunopositive neurons being found throughout both laminae (Figure 8(f)).

3.3.3 | The medial amygdaloid nucleus

The medial amygdaloid nucleus occupied the most medial aspect of the amygdaloid body (Figures 2(g)–2(j)) and we could identify both the dorsal (Mcd) and ventral (Mcv) subdivisions of this nucleus in the tree pangolin. The medial amygdaloid nucleus could be readily distinguished from the adjacent PACm through the absence of parvalbumin and neurofilament H-immunostained structures (Figures 8(d) and 8(g)), as well as a greater density of calretinin-immunopositive structures

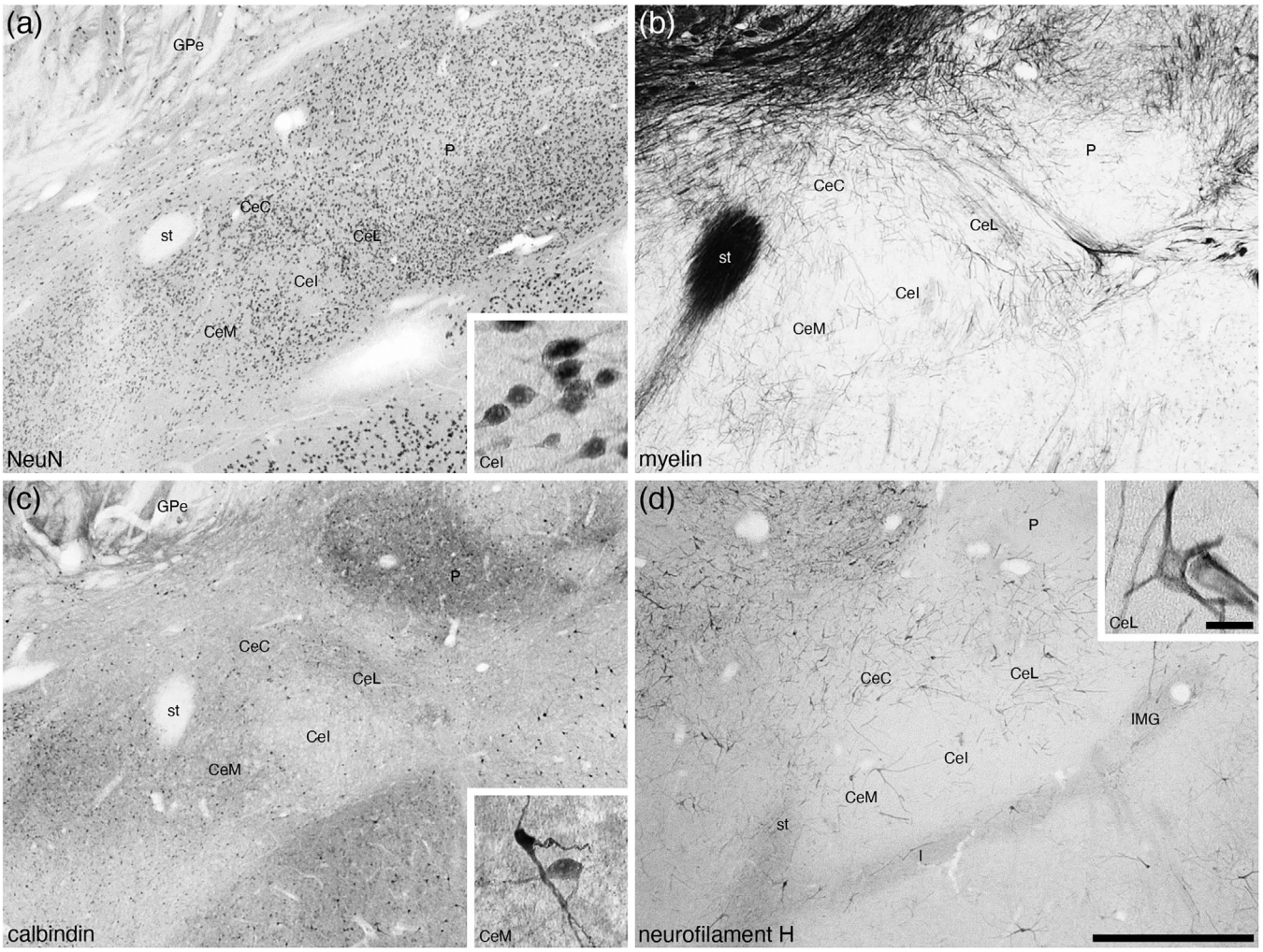

FIGURE 7 Low magnification photomicrographs of the central nuclear cluster within the amygdaloid body of the tree pangolin stained for neuronal nuclear marker (NeuN, a), myelin (b), calbindin (c), and neurofilament H (d). Although the architectonic delineation into distinct subnuclei is not always unambiguous, we could identify with reasonable certainty the medial (CeM), intermediate (CeI), lateral (CeL), and capsular (CeC) divisions of the central nuclear cluster of the centromedial group. In all images, dorsal is to the top and medial to the left. Scale bar in (d) = 1 mm and applies to all. Scale bar inset (d) = 25 μm and applies to all insets. See list for abbreviations

(Figure 8(f)). While the laminar borders within both these subdivisions were not sharp, we could identify three layers (Figure 8). In both the Mcd and Mcv, the most superficial layer, layer 1, showed a very low density of neurons (Figures 8(a)–8(c)), but no differences between the two subdivisions were observed with any stains used in the current study (Figures 8(b)–8(g)). Layer 2 in both subdivisions housed the highest density of neurons, with the Mcv appearing to have a higher density of intensely neuronal nuclear marker-immunoreactive neurons within this layer when compared with layer 2 of the Mcd (Figures 8(a)–8(c)). A higher density of calbindin-immunopositive neurons, as well as a more intense calbindin-immunostained neuropil in layer 2 distinguished Mcd from Mcv (Figure 8(e)), while no distinct difference in calretinin-immunostaining between the two subdivision is evident in layer 2 (Figure 8(f)). Layer 3 of both subdivisions exhibited a lower density of neurons than layer 2, and the density of these neurons decreased with depth in the layer (Figures 8(b) and 8(c)). No distinct differences in the chemoarchitecture of layer 3 were evident that contributed to the delineation of these two subdivisions (Figures 8(d)–8(g)). Thus, while we identify two subdivisions of the medial amygdaloid nucleus the differences between these subdivisions are subtle.

3.4 | Other amygdaloid nuclei

3.4.1 | The AAA

The AAA was located on the medial aspect of the anterior portion of the amygdaloid body, lying between the ventral pallidum (VP) and the nucleus of the lateral olfactory tract (NLOT) (Figures 2(a)–2(d) and 9). This moderately neuron-dense area (Figure 9(a)) was readily distinguished from the VP medially and NLOT laterally by the absence of distinct immunostaining for choline acetyltransferase (Figure 9(b)), a

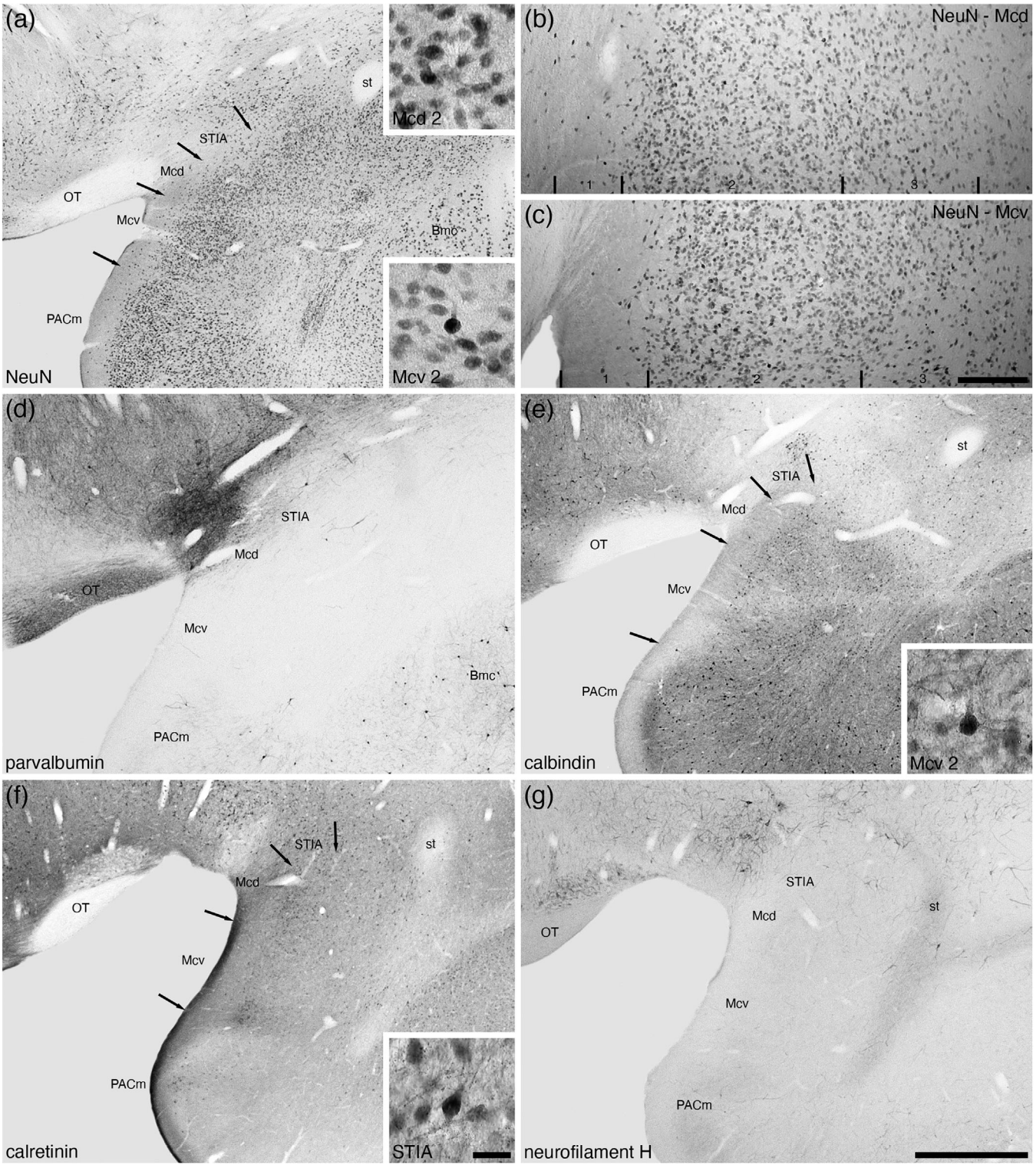

FIGURE 8 Low and higher magnification photomicrographs of the medial amygdaloid nucleus within the amygdaloid body of the tree pangolin stained for neuronal nuclear marker (NeuN, a, b, c), parvalbumin (d), calbindin (e), calretinin (f), and neurofilament H (g). We observed both dorsal (Mcd) and ventral (Mcv) subdivisions of the medial amygdaloid nucleus, as well as the intramygdaloid division of the bed nucleus of the stria terminalis (STIA). Both Mcd and Mcv evinced three layer (1, 2, 3) (b, c), although the laminar borders were not sharp. The insets in (a) are high magnification images of NeuN immunostained neurons in layer 2 of the Mcd and Mcv, the inset in (e) is of calbindin immunostained neurons in layer 2 of the Mcv, and the inset in (f) is of calretinin immunostained neurons in the STIA. In all images, dorsal is to the top and medial to the left. Scale bar in (g) = 1 mm and applies to (a), (d)–(g). Scale bar in (c) = 200 μm and applies to (b) and (c). Scale bar in inset (f) = 25 μm and applies to all insets. See list for abbreviations

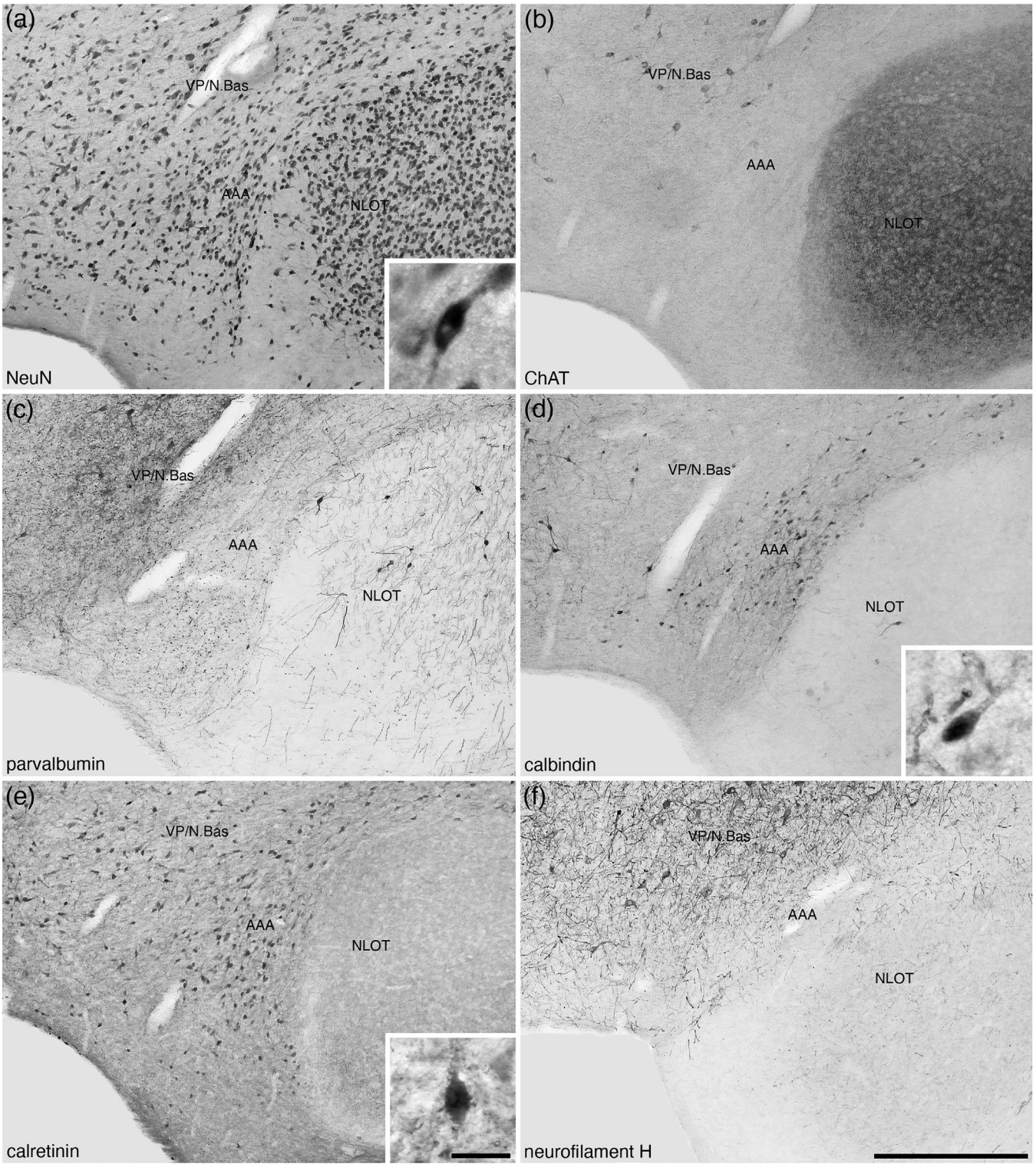

FIGURE 9 Lower (a–f) and higher (insets a, d, e) magnification photomicrographs of the anterior amygdaloid area (AAA) of the amygdaloid body of the tree pangolin stained for neuronal nuclear marker (NeuN, a), cholineacetyltransferase (ChAT, b), parvalbumin (c), calbindin (d), calretinin (e), and neurofilament H (f). The insets are high magnification images of immunostained neurons in the AAA (NeuN—inset a, calbindin—inset c, and calretinin—inset d). In all images, dorsal is to the top and medial to the left. Scale bar in (f) = 500 μm and applies to (a)–(f). Scale bar in inset (e) = 25 μm and applies to all insets. See list for abbreviations.

significantly lower density of parvalbumin-immunopositive structures than the VP, and the presence of parvalbumin-immunopositive neurons in the NLOT (Figure 9(c)). In addition, a moderate density of calbindin-immunopositive neurons were observed in the AAA, which exhibited a much lower density in the VP and were almost absent in the NLOT (Figure 9(d)). A moderate density of calretinin-immunopositive neurons were observed in the AAA, with these neurons being absent in the NLOT and of a lower density in the VP (Figure 9(e)). A high density of neurofilament H-immunopositive soma and dendrites characterized the VP, while in the AAA, the immunopositive soma were absent and a much lower density of dendrites were observed, both of which are absent in the NLOT (Figure 9(f)). This combination of features allowed the delineation of the AAA from surrounding structures.

3.4.2 | The IMG and I

The IMG in the brain of the tree pangolin was observed to lie between the lateral amygdaloid nucleus and the putamen (Figures 2(f)–2(h) and 10). Unlike the isolated intercalated cell masses reported in certain other species (e.g., Paxinos et al., 2009; Limacher-Burrell et al., 2016, 2018; but see Marowsky et al., 2005; Pinard et al., 2012, for a more comprehensive description of these nuclei in the rat amygdaloid body where there are similarities to what is observed in the tree pangolin), the I within the tree pangolin was composed of a single band lying between the basal and central amygdaloid nuclei (Figures 2(f)–2(i) and 10). The architecture and chemoarchitecture of both the IMG and I bands in the tree pangolin were very similar. In both the IMG and I bands, there was a high density of small neurons, with this density being slightly higher in the I when compared directly with the IMG (Figures 10(a), 10(e), and 10(h)). In both the IMG and I, calbindin-immunopositive neurons were observed, and these appeared to be quite similar in terms of density and neuronal types (Figure 10(b), 10(f), and 10(i)). In both the IMG and I, there was a conspicuous absence of calretinin immunostaining (Figure 10(c)), while a distinct neuropil neurofilament H-immunopositive staining was observe in both (Figure 10(d)). A moderately dense tyrosine hydroxylase-immunopositive terminal network was observed in both the IMG and I, with this terminal network appearing to be slightly more dense in the IMG (Figures 10(g) and 10(j)). The other stains used in the current study did not reveal any additional structures in either the IMG or I.

3.4.3 | The AHiA

The AHiA was observed at the caudal pole of the amygdaloid body, at the transition between the amygdalioid body and the hippocampal formation (Figures 2(k) and 2(l)). The AHiA exhibited a slightly lower neuronal density than surrounding structures (Figure 11(a)), with a lower density of parvalbumin-immunopositive neurons, dendrites and neuropil (Figure 11(b)). A lower density of calbindin- and calretinin-immunopositive neurons were observed in the AHiA compared with surrounding structures (Figures 11(c) and 11(d)), as well as a less intense calretinin-immunopositive neuropil staining that the dorsally located basal amygdaloid nucleus (Figure 11(d)).

4 | DISCUSSION

The amygdaloid complex, being responsible for the generation of affective states/emotions in relation to stimuli relevant to the survival of individuals as members of a particular species (e.g., Rolls, 1999; Panskepp, 2011), is an important structure within the brain of all vertebrates. Despite the species-specificity of the stimuli that generate affective states, cross-species comparisons of the nuclear organization of the amygdaloid body of mammals has revealed only minor variations (e.g., Fox, 1940; Krettek & Price, 1978; Price et al., 1987; Pitkänen & Amaral, 1993a, b; Pitkänen et al., 1997; Kemppainen & Pitkänen, 2000; Ashwell, 2010; Limacher-Burrell et al., 2016, 2018; Pillay et al., 2021). The tree pangolin is not an exception to this conserved structural organization, and in the current study, we could readily determine the organization of the tree pangolin amygdaloid body by relating our observations to studies in other mammals. In this sense, while the stimuli that evoke affective state generation by the amygdaloid body the tree pangolin may differ to other species, it appears that the broad neuronal circuits that process these stimuli, and initiate affective states and behaviors, are conserved across mammalian brains.

4.1 | Pangolin and carnivore amygdalae—similarities and differences

As the Philodota (or Manidae) and Carnivora are considered sister-orders within the Laurasiatherian mammal radiation (Arnason et al., 2008; Yu et al., 2011; Foley et al., 2016), we compared the results of our analysis to similar studies undertaken in carnivores to determine whether we could reveal any derived traits of the tree pangolin amygdaloid body in comparison with their closest relatives. Architectonic analyses of the amygdaloid body among the carnivores are available for the domestic dog (Kosmal & Nitecka, 1977), domestic cat (Fox, 1940), domestic ferret, and banded mongoose (Pillay et al., 2021). The general pattern of main nuclear subdivisions and compartmentalization of these subdivisions is shared across the species for which data are available. There does not appear to be any specific variances in the general organization of the tree pangolin amygdala that is not readily observed in the carnivoran amygdala. This indicates the likelihood that the neural processing and generation of affect-laden stimuli and affect-driven behavior is similar across these related species. The sole difference of note when comparing the tree pangolin amygdala to that of carnivores is the dorsal extension of the CoA and the deep involution of the NLOT within the tree pangolin amygdaloid body that is not seen in the carnivores that have been studied (Kosmal & Nitecka, 1977; Fox, 1940; Pillay et al., 2021). This potentially indicates a shift toward more of the amygdaloid body being devoted to the processing of affect related to olfactory information than might be observed in carnivores, although

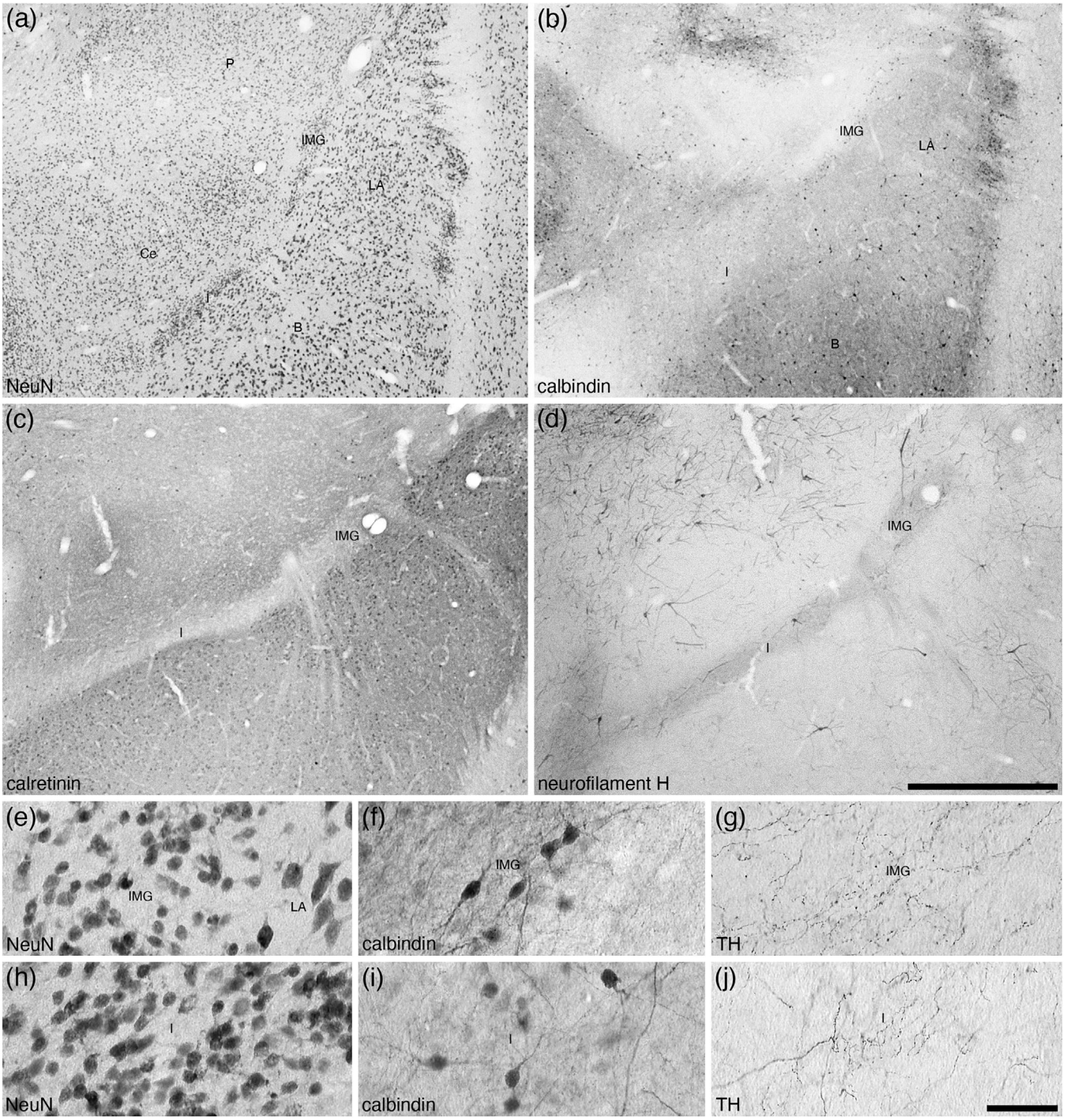

FIGURE 10 Lower (a–d) and higher (e–j) magnification photomicrographs of the amygdaloid intramedullary gray matter (IMG) and intercalated island, or band, of the amygdala (I) within the amygdaloid body of the tree pangolin stained for neuronal nuclear marker (NeuN, a, e, h), calbindin (b, f, i), calretinin (c), neurofilament H (d), and tyrosine hydroxylase (g, j). Note how both the IMG and I form distinct bands of small neurons (e, h) between the lateral amygdaloid nucleus and putamen (IMG) and basal amygdaloid nucleus and central amygdaloid nucleus (I). Note the specific absence of calretinin immunostaining in these nuclei (c), and the marked neuropil staining for neurofilament H in both nuclei (d). Some of these neurons are immunopositive for calbindin (f, i), and in both the IMG and I there is a moderately dense tyrosine hydroxylase immunopositive terminal network (g, j). In all images, dorsal is to the top and medial to the left. Scale bar in (d) = 1 mm and applies to (a)–(d). Scale bar in (j) = 50 μm and applies to (e)–(j). See list for abbreviations

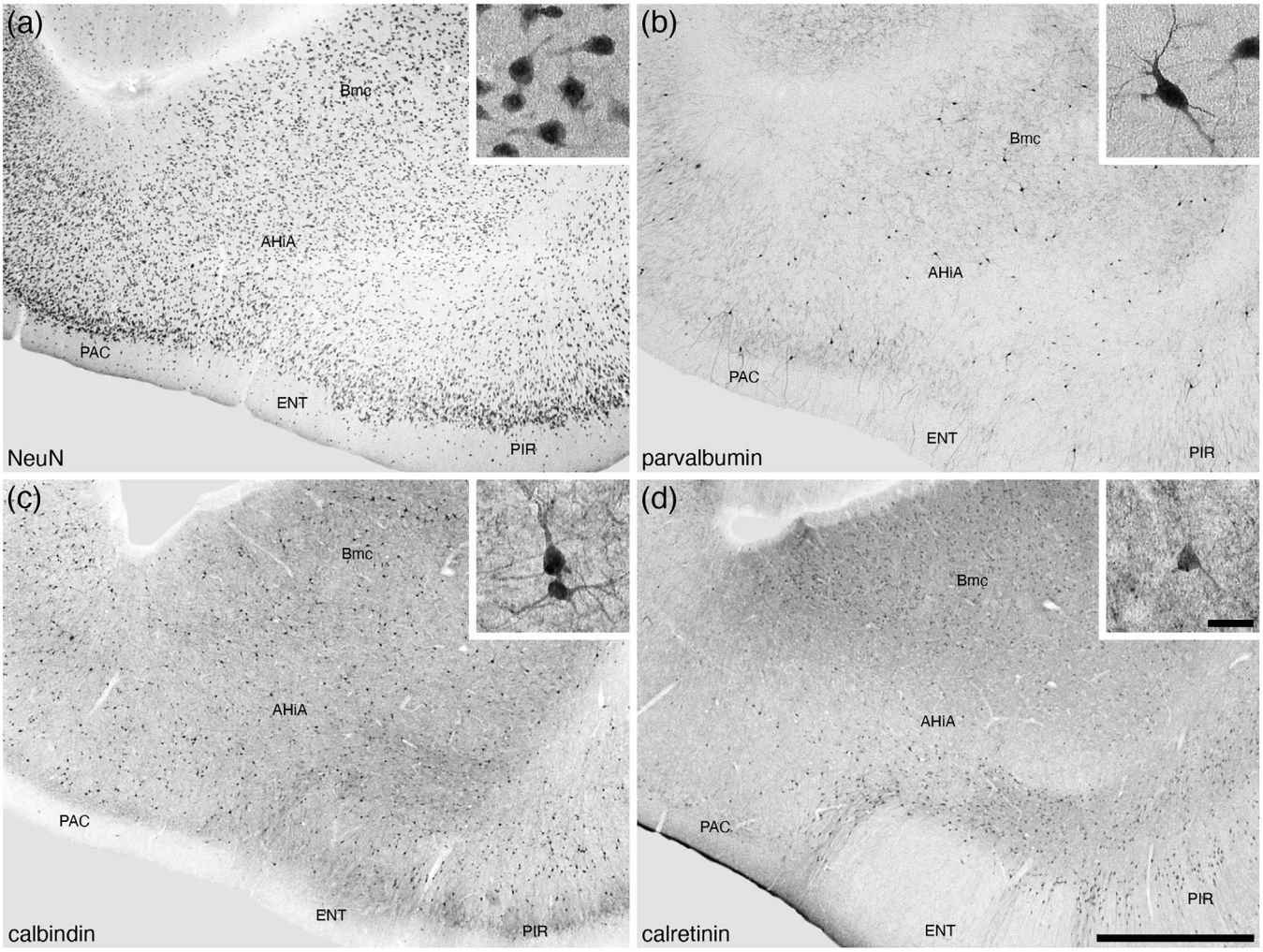

FIGURE 11 Lower (a–d) and higher (insets of a–d) magnification photomicrographs of the amygdalohippocampal area (AHiA) of the amygdaloid body of the tree pangolin stained for neuronal nuclear marker (NeuN, a), parvalbumin (b), calbindin (c), and calretinin (d). The insets are high magnification images of immunostained neurons in the CeI (NeuN, inset a), CeM (calbindin, inset c), and CeL (neurofilament H, inset d). In all images, dorsal is to the top and medial to the left. Scale bar in (d) = 1 mm and applies to (a)–(d). Scale bar in inset (d) = 25 μm and applies to all insets. See list for abbreviations.

this would require further investigation to determine the validity of this possibility.

4.2 | Broad similarities of amygdaloid body organization across mammals

The similarity of the organization of the amygdaloid body in pangolins and carnivores extends more broadly across mammals. In the mammal species that have been studied, the main nuclear groupings (such as lateral, basal, basal accessory, cortical, centromedial and other nuclei) appear to be present, as well as the internal divisions of these groups (e.g., sheep—Richard, 1967; laboratory rat—Krettek & Price, 1978, Pitkänen et al., 1997, Kemppainen & Pitkänen, 2000; crab-eating macaque—Pitkänen & Amaral, 1993a, b; tree shrew—Flügge et al., 1994; human—Sorvari et al., 1995; rabbit—Jagalska-Majewska et al., 2001; horse, cow, and pig—Takeuchi & Sugita, 2007; opossum—Rocha-Rego et al., 2008; rock hyrax—Limacher-Burrell et al., 2016; African elephant—Limacher-Burrell et al., 2018). This broad similarity in the organization of the amygdaloid body across species indicates that the neural processing of information relevant to affect is organized along similar pathways and networks across species, the closer study of which may allow for the definition and possible inference of homology of specific affect states across mammals; however, this would require extensive physiological and behavioral studies to determine if this can be achieved.

Despite these broad similarities, there was one specific feature of the tree pangolin amygdaloid body, which appears to be shared by the carnivores, and partially by laboratory rats (Marowsky et al., 2005; Pinard et al., 2012), that was noted to be somewhat different to that observed in other mammal species. In the tree pangolin, the IMG and the intercalated islands (I) evince a very similar architecture

and immunostaining pattern, as well as these neuronal clusters being located very close to each other. In addition, in the tree pangolin, the intercalated islands do not appear to be distinct islands, rather they have an appearance that does not differ from the IMG. In the domestic cat (Fox, 1940), domestic dog (Kosmal & Nitecka, 1977), domestic ferret, and banded mongoose (Pillay et al., 2021), and partially in laboratory rats (Marowsky et al., 2005; Pinard et al., 2012), a somewhat similar nonisolated architectural pattern of portions of the intercalated islands is depicted. In these species, the intercalated islands are located dorsomedial to the basolateral group. In contrast, in other studies of the laboratory rat (Krettek & Price, 1978; Pitkänen et al., 1997; Kemppainen & Pitkänen, 2000), crab-eating macaque (Pitkänen & Amaral, 1993a, b), human (Sorvari et al., 1995), rock hyrax (Limacher-Burrell et al., 2016), and African elephant (Limacher-Burrell et al., 2018), the intercalated islands are distinct islands, rather than a "band" of neurons, and are often located between the basal and accessory basal nuclei. These intercalated neurons play a role in the control of inhibition in the central amygdaloid nucleus (Sah et al., 2003), and thus may contribute to the modulation of fear conditioning. The observed differences in the architectural organization of the intercalated amygdaloid neurons between species may play a role in the differential expression and conditioning of fear responses in different species, but this possibility requires further study.

4.3 | Are there any potentially adaptive aspects regarding affect in pangolins?

The range of affective behaviors observed in captive pangolins, as outlined by Mohapatra & Panda (2014) and Zhang et al. (2020), has been observed in many other mammalian species. In this sense, given the conserved organization of the amygdaloid body in the tree pangolin in comparison with other mammals, as determined with the methods employed in the current study, it would be difficult at this stage to posit any species-specific specializations of the neural processing and subsequent behavioral expression of affect in the tree pangolin. Directed studies of other aspects of amygdaloid organization in the tree pangolin may reveal clues to lineage or species-specific neural processing of affect, such as has been observed regarding the expression of aggression (Jacobs et al., 2006) or domestication (Saetre et al., 2004) in the domestic dog.

Despite these potential avenues, perhaps the most direct way to further develop our understanding of affect in the tree pangolin would be through the identification of the specific sensory stimuli that initiate affective behaviors. The investigation of such stimuli, involved in reproduction, fear, aggression, and other affective behaviors, would augment our understanding of these unusual mammalian species and may lead to better husbandry practices as well as improving, or developing, the possibility of captive breeding colonies to assist in the reintroduction of pangolin species where wild populations have been eliminated due to poaching and human encroachment on natural habitats.

ACKNOWLEDGMENTS

We thank Dr. Elizabeth Ebewele of the Department of Forestry, Federal Ministry of Environment, Nigeria, for her assistance in helping to facilitate the issuance of the CITES permit.

CONFLICT OF INTEREST

The authors declare no conflicts of interest.

AUTHOR CONTRIBUTIONS

P. R. M. conceptualized the study. A. I., A. B., M. S. A., and P. R. M. obtained the brains. A. I., A. B., and P. R. M. performed the staining and analysis. A. I. and P. R. M. wrote the manuscript, and the remaining authors contributed to the editing and improvement of the early drafts of the manuscript. All authors had full access to all data in the study and take responsibility for the integrity of the data and the accuracy of the data analysis.

DATA AVAILABILITY STATEMENT

Data have not been shared due to this study being based on histological sections.

TRANSPARENT PEER REVIEW

The peer review history for this article is available at https://publons.com/publon/10.1002/cne.25345

REFERENCES

Adrio, F., Rodriguez-Moldes, I., & Anadon, R. (2011). Distribution of glycine immunoreactivity in the brain of the Siberian sturgeon (*Acipenser baeri*): Comparison with γ-aminobutyric acid. *Journal of Comparative Neurology*, *519*, 1115–1142. https://doi.org/10.1002/cne.22556

Alheid, G. F. (2003). Extended amygdala and basal forebrain. *Annals of the New York Academy of Sciences*, *985*, 185–205. https://doi.org/10.1111/j.1749-6632.2003.tb07082.x

Arnason, U., Adegoke, J. A., Gullberg, A., Harley, E. H., Janke, A., & Kullberg, M. (2008). Mitogenomic relationships of placental mammals and molecular estimates of their divergences. *Gene*, *421*, 37–51. https://doi.org/10.1016/j.gene.2008.05.024

Ashwell, K. W. S. (2010). *The neurobiology of Australian Marsupials. Brain evolution in the other mammalian radiation*. Cambridge, UK: Cambridge University Press.

Brown, J. P., Couillard-Despres, S., Cooper-Kuhn, C. M., Winkler, J., Aigner, L., & Kuhn, H. G. (2003). Transient expression of doublecortin during adult neurogenesis. *Journal of Comparative Neurology*, *467*, 1–10. https://doi.org/10.1002/cne.10874

Bunce, J. G., Zikopoulos, B., Feinberg, M., & Barbas, H. (2013). Parallel prefrontal pathways reach distinct excitatory and inhibitory systems in memory-related rhinal cortices. *Journal of Comparative Neurology*, *521*, 4260–4283. https://doi.org/10.1002/cne.23413

de Olmos, J. S., Beltramino, C. A., & Alheid, C. (2004). Amygdala and extended amygdala of the rat: A cytoarchitectonical, fibroarchitectonical, and chemoarchitectonical survey. In G. Paxinos (Ed.), *The rat nervous system*, Third Edition (pp. 509–603). Amsterdam: Elsevier-Academic Press.

Flügge, G., Ahrens, O., & Fuchs, E. (1994). Monoamine receptors in the amygdaloid complex of the tree shrew (*Tupaia belangeri*). *Journal of Comparative Neurology*, *343*, 597–608. https://doi.org/10.1002/cne.903430409

Foley, N. M., Springer, M. S., & Teeling, E. C. (2016). Mammal madness: Is the mammal tree of life not yet resolved? *Philosophical Transactions of*

the Royal Society of London. Series B, Biological Sciences, *317*, 20150140. https://doi.org/10.1098/rstb.2015.0140

Fox, C. A. (1940). Certain basal telencephalic centers in the cat. *Journal of Comparative Neurology*, *72*, 1–62. https://doi.org/10.1002/cne.900720102

Griffin, G. D., Ferri-Kolwicz, S. L., Reyes, B. A. S., van Bockstaele, E. J., & Flanagan-Cato, L. M. (2010). Ovarian hormone-induced reorganization of oxytocin-labeled dendrites and synpases lateral to the hypothalamic ventromedial nucleus in female rats. *Journal of Comparative Neurology*, *518*, 4531–4545. https://doi.org/10.1002/cne.22470

Hirano, A. A., Brandstatter, J. H., Morgans, C. W., & Brecha, N. C. (2011). SNAP25 expression in mammalian retinal horizontal cells. *Journal of Comparative Neurology*, *519*, 972–988. https://doi.org/10.1002/cne.22562

Imam, A., Ajao, M. S., Bhagwandin, A., Ihunwo, A. O., & Manger, P. R. (2017). The brain of the tree pangolin (*Manis tricuspis*). I. General appearance of the central nervous system. *Journal of Comparative Neurology*, *525*, 2571–2582. https://doi.org/10.1002/cne.24222

Imam, A., Bhagwandin, A., Ajao, M. S., Spocter, M. A., Ihunwo, A. O., & Manger, P. R. (2018a). The brain of the tree pangolin (*Manis tricuspis*). II. The olfactory system. *Journal of Comparative Neurology*, *526*, 2548–2569. https://doi.org/10.1002/cne.24510

Imam, A., Bhagwandin, A., Ajao, M. S., Ihunwo, A. O., Fuxe, K., & Manger, P. R. (2018b). Brain of the tree pangolin (*Manis tricuspis*). III. The unusual locus coeruleus complex. *Journal of Comparative Neurology*, *526*, 2570–2584. https://doi.org/10.1002/cne.24519

Imam, A., Bhagwandin, A., Ajao, M. S., Ihunwo, A. O., & Manger, P. R. (2019a). The brain of the tree pangolin (*Manis tricuspis*). IV. The hippocampal formation. *Journal of Comparative Neurology*, *527*, 2393–2412. https://doi.org/10.1002/cne.24519

Imam, A., Bhagwandin, A., Ajao, M. S., & Manger, P. R. (2019b). The brain of the tree pangolin (*Manis tricuspis*). V. The diencephalon and hypothalamus. *Journal of Comparative Neurology*, *527*, 2413–2439. https://doi.org/10.1002/cne.24619

Imam, A., Bhagwandin, A., Ajao, M. S., Spocter, M. A., & Manger, P. R. (2019c). The brain of the tree pangolin (*Manis tricuspis*). V. The brainstem and cerebellum. *Journal of Comparative Neurology*, *527*, 2440–2473. https://doi.org/10.1002/cne.24721

Jacobs, C., van den Broeck, W., & Simoens, P. (2006). Neurokinin-1 receptor in the basolateral nuclear group of the canine amygdala – comparative study in normal and aggressive dogs. *Brain Research*, *1098*, 106–122. https://j.brainres.2006.04.099

Jagalska-Majewska, H., Dziewiątkowski, J., Wójik, S., Łuczynska, A., Kurlapska, R., & Moryś, J. (2001). The amygdaloid complex of the rabbit – morphological and histochemical study. *Folia Morphologica*, *60*, 259–280.

Kaiser, A., Alexandrova, O., & Grothe, B. (2011). Urocortin-expressing olivocochlear neurons exhibit tonotopic and developmental changes in the auditory brainstem and in the innervation of the cochlea. *Journal of Comparative Neurology*, *519*, 2758–2778. https://doi.org/10.1002/cne.22650

Kemppainen, S., & Pitkänen, A. (2000). Distribution of parvalbumin, calretinin and calbindin-D28 k immunoreactivity in the rat amygdaloid complex and colocalization with gamma-aminobutyric acid. *Journal of Comparative Neurology*, *426*, 441–467. https://doi.org/10.1002/1096-9861(20001023)426:3<441::aid-cne8>3.0.co;2-7

Kosmal, A., & Nitecka, L. (1977). Cytoarchitecture and acetylcholinesterase activity of the amygdaloid nuclei in the dog. *Acta Neurobiologiae Experimentalis*, *37*, 363–374.

Krettek, J. E., & Price, J. L. (1978). A description of the amygdaloid complex in the rat and cat with observations on intra-amygdaloid axonal connections. *Journal of Comparative Neurology*, *178*, 255–280. https://doi.org/10.1002/cne.901780205

Laux, A., Delalande, F., Mouheiche, J., Stuber, D., van Dorsselaer, A., Bianchi, E., Bezard, E., & Goumon, Y. (2012). Localization of endogenous morphine-like compounds in the mouse spinal cord. *Journal of Comparative Neurology*, *520*, 1547–1561. https://doi.org/10.1002/cne.22811

Li, S., & Kiruoac, J. (2008). Projections from the paraventricular nucleus of the thalamus to the forebrain, with special emphasis on the extended amygdala. *Journal of Comparative Neurology*, *506*, 263–287. https://doi.org/10.1002/cne.21502

Limacher-Burrell, A. M., Bhagwandin, A., Gravett, N., Maseko, B. C., & Manger, P. R. (2016). Nuclear organization of the rock hyrax (*Procavia capensis*) amygdaloid body. *Brain Structure and Function*, *221*, 3171–3191. https://doi.org/10.1007/s00429-015-1094-8

Limacher-Burrell, A. M., Bhagwandin, A., Maseko, B. C., & Manger, P. R. (2018). Nuclear organization of the African elephant (*Loxodonta africana*) amygdaloid complex: An unusual mammalian amygdala. *Brain Structure and Function*, *223*, 1191–1216. https://doi.org/10.1007/s00429-017-1555-3

Marowsky, A., Yanagawa, Y., Obata, K., & Vogt, K. E. (2005). A specialized subclass of interneurons mediates dopaminergic facilitation of amygdala function. *Neuron*, *48*, 1025–1037. https://doi.org/10.1016/j.neuron.2005.10.029

Mohapatra, R. K., & Panda, S. (2014). Behavioural descriptions of Indian pangolins (*Manis crassicaudata*) in captivity. *International Journal of Zoology*, *2014*, 795062. http://doi.org/10.1155/2014/795062

Ngwenya, A., Patzke, N., Manger, P. R., & Herculano-Houzel, S. (2016). Continued growth of the central nervous system without mandatory addition of neurons in the Nile crocodile (*Crocodylus niloticus*). *Brain, Behavior and Evolution*, *87*, 19–38. https://doi.org/10.1159/000443201

Panksepp, J. (2011). The basic emotional circuits of mammalian brains: Do animals have affective lives? *Neuroscience and Biobehavioral Reviews*, *35*, 1791–1804. https://doi.org/10.1016/j.neubiorev.2011.08.003

Patzke, N., Spocter, M. A., Karlsson, K. Æ., Bertelsen, M. F., Haagensen, M., Chawana, R., Streicher, S., Kaswera, C., Gilissen, E., Alagaili, A. N., Mohammed, O. B., Reep, R. L., Bennett, N. C., Siegel, J. M., Ihunwo, A. O., & Manger, P. R. (2015). In contrast to many other mammals, cetaceans have relatively small hippocampi that appear to lack adult neurogenesis. *Brain Structure and Function*, *220*, 361–383. https://doi.org/10.1007/s00429-013-0660-1

Paxinos, G., Watson, C., Carrive, P., Kirkcaldie, M. T. K., & Ashwell, K. (2009). *Chemoarchitectonic Atlas of the Rat Brain*. New York: Elsevier.

Pillay, S., Bhagwandin, A., Bertelsen, M. F., Patzke, N., Engler, G., Engel, A. K., & Manger, P. R. (2021). The amygdaloid body of two carnivore species: The feliform banded mongoose and the caniform domestic ferret. *Journal of Comparative Neurology*, *529*, 28–51. https://doi.org/10.1002/cne.25046

Pinard, C. R., Mascagni, F., & McDonald, A. J. (2012). Medial prefrontal cortical innervation of the intercalated nuclear region of the amygdala. *Neuroscience*, *205*, 112–124. https://doi.org/10.1016/j.neuroscience.2011.12.036

Piskuric, N. A., Vollmer, C., & Nurse, C. A. (2011). Confocal immunofluorescence study of rat aortic body chemoreceptors and associated neurons *in situ* and *in vitro*. *Journal of Comparative Neurology*, *519*, 856–873. https://doi.org/10.1002/cne.22553

Pitkänen, A., & Amaral, D. G. (1993a). Distribution of parvalbumin immunoreactive cells and fibers in the monkey temporal lobe: The amygdaloid complex. *Journal of Comparative Neurology*, *331*, 14–36. https://doi.org/10.1002/cne.903310103

Pitkänen, A., & Amaral, D. G. (1993b). Distribution of calbindin-D28k immunoreactivity in the monkey temporal lobe: The amygdaloid complex. *Journal of Comparative Neurology*, *331*, 199–224. https://doi.org/10.1002/cne.903310205

Pitkänen, A., Savander, V., & LeDoux, J. E. (1997). Organization of intraamygdaloid circuitries in the rat: An emerging framework for understanding functions of the amygdala. *Trends in Neuroscience*, *20*, 517–523. https://doi/org/10.1016/s0166-2236(97)01125-9

Price, J. L., Russchen, F. T., & Amaral, D. G. (1987). The limbic region. II. The amygdaloid complex. In: A. Bjorklund, T. Hokfelt, & L.W. Swanson (Eds.), *Handbook of Chemical Neuroanatomy, Volume 5, Integrated Systems of the CNS, Part 1* (pp. 279–381). Amsterdam: Elsevier Science.

Puelles, L. (2017). Comments on the updated tetrapartite pallium model in the mouse and chick, featuring a homologous claustro-insular complex. *Brain, Behavior and Evolution*, *90*, 171–189. https://doi.org/10.1159/000479782

Radtke-Schuller, S. (2018). *Cyto- and Myeloarchitectural Brain Atlas of the Ferret (Mustela putorius) in MRI Aided Stereotaxic Coordinates*. Switzerland: Springer International Publishing AG.

Richard, P. (1967). *Atlas Stéréotaxique Du Cerveau de Brebis*. Paris: INRA.

Rocha-Rego, V., Canteras, N. S., Anomal, R. F., Volchan, E., & Franca, J. G. (2008). Architectonic subdivisions of the amygdalar complex of a primitive marsupial (*Didelphis aurita*). *Brain Research Bulletin*, *76*, 26–35. https://doi.org/10.1016/j.brainresbull.2008.01.004

Rolls, E. T. (1999). *The Brain and Emotion*. Oxford, UK: Oxford University Press.

Rubenstein, D. I., & Wrangham, R. W. (2014). *Ecological Aspects of Social Evolution. Birds and Mammals*. Princeton, NJ: Princeton University Press.

Saetre, P., Lindberg, J., Leonard, J. A., Olsson, K., Pettersson, U., Ellegran, H., Bergström, T. F., Vilà, C., & Jazin, E. (2004). From wild wolf to domestic dog: Gene expression changes in the brain. *Molecular Brain Research*, *126*, 198–206. https://doi.org/10.1016/j.molbrainres.2004.05.003

Sah, P., Faber, E. S. L., Lopez de Armentia, M., & Power, J. (2003). The amygdaloid complex: Anatomy and physiology. *Physiological Reviews*, *83*, 803–834. https://doi.org/10.1152/physrev.00002.2003

Sorvari, H., Soininen, H., Paljärvi, L., Karkola, K., & Pitkänen, A. (1995). Distribution of parvalbumin-immunoreactive cells and fibers in the human amygdaloid complex. *Journal of Comparative Neurology*, *360*, 185–212. https://doi.org/10.1002/cne.903600202

Sternberger, L. A., & Sternberger, N. H. (1983). Monoclonal antibodies distinguish phosphorylated and nonphosphorylated forms of neurofilaments *in situ*. *Proceedings of the National Academy of Science of the United States of America*, *80*, 6126–6130. https://doi.org/10.1073/pnas.80.19.6126

Takeuchi, T., & Sugita, S. (2007). Histological atlas and morphological features by Nissl staining in the amygdaloid complex of the horse, cow and pig. *Journal of Equine Science*, *18*, 13–25. https://doi.org/10.1294/jes.18.13

Watson, C., Mitchelle, A., & Puelles, L. (2017). A new mammalian brain ontology based on developmental gene expression. In J. H. Kaas (Ed.), *Evolution of Nervous Systems*, 2nd Edition (pp. 53–75). Oxford: Elsevier.

Wong, P., Gharbawie, O. A., Luethke, L. E., & Kaas, J. H. (2008). Thalamic connections of architectonic subdivisions of temporal cortex in grey squirrels (*Sciurus carolinensis*). *Journal of Comparative Neurology*, *510*, 440–461. https://doi.org/10.1002/cne.21805

Yu, H. T., Ma, G. C., Lee, D. J., Chin, S. C., Tsao, H. S., Wu, S. H., Shih, S. Y., & Chen, M. (2011). Molecular delineation of the Y-borne *Sry* gene in the Formosan pangolin (*Manis pentadactyla pentadactyla*) and its phylogenetic implications for Pholidota in extant mammals. *Theriogenology*, *75*, 55–64. https://j.theriogenology.2010.07.010

Zhang, F., Yu, Y., Yu, J., Wu, S., Li, S., Wang, Q., Min, Y., & Sun, R. (2020). Reproductive behavior of the captive Sunda pangolin (*Manis javanica* Desmarest, 1822). *Zoo Biology*, *39*, 65–72. https://doi.org/10.1002/zoo.21526

How to cite this article: Imam, A., Bhagwandin, A., Ajao, M. S., & Manger, P. R. (2022). The brain of the tree pangolin (*Manis tricuspis*). VII. The amygdaloid body. *Journal of Comparative Neurology*, *530*, 2590–2610. https://doi.org/10.1002/cne.25345